Andreev states, supercurrents and interface effects in clean superconducting/normal metal multilayers

2003 J. Phys.: Condens. Matter 15 1847

(http://iopscience.iop.org/0953-8984/15/12/304)

INSTITUTE OF PHYSICS PUBLISHING JOURNAL OF PHYSICS: CONDENSED MATTER

J. Phys.: Condens. Matter **15** (2003) 1847–1878 PII: S0953-8984(03)57018-7

Andreev states, supercurrents and interface effects in clean superconducting/normal metal multilayers

C Ciuhu, A Lodder[1], R E S Otadoy and R T W Koperdraad

Faculty of Sciences/Natuurkunde en Sterrenkunde, Vrije Universiteit, De Boelelaan 1081, 1081 HV Amsterdam, The Netherlands

E-mail: alod@nat.vu.nl

Received 2 December 2002
Published 10 March 2003
Online at stacks.iop.org/JPhysCM/15/1847

Abstract

We present results for the local density of states in the superconducting (S) and normal metallic (N) layers of an SN multilayer, and the supercurrent, based on a Green function formalism, as an extension of previous calculations on NS, SNS and SNSNS systems. The gap function is determined self-consistently. Our systems are chosen to have a finite transverse width. We focus on phenomena which occur at so-called critical transverse widths, at which a new transverse mode is starting to contribute. It appears that for an arbitrary width the Andreev approximation (AA), which takes into account only Andreev reflection at the SN interfaces, works well. We show that at a critical width the AA breaks down. An exact treatment is required, which also considers ordinary reflections. In addition, we study the influence of an interface barrier on the coupling between the S layers.

1. Introduction

Starting about two decades ago, the interest of developing devices at a very small scale gave rise to a new branch in physics, mesoscopic physics. Both theoretically and experimentally, many interesting phenomena were discovered that occur at this scale which lies essentially in the submicron ranges.

Many samples are built up of superconducting (S) and normal metallic (N) components in which necessarily SN interfaces and possibly point contacts occur. This is why a lot of theoretical work was devoted to studying different SN configurations.

The first experimental investigations, using tunnelling spectroscopy measurements, revealed the fact that the density of states in a normal metal connected to a superconductor is modified [1]. McMillan provided a simple tunnelling model for the proximity effect at SN interfaces, which allows for a solution of the Gor'kov equations. Ishii [2] and Furusaki *et al* [3, 4] extended his work to include Andreev reflections.

[1] Author to whom any correspondence should be addressed.

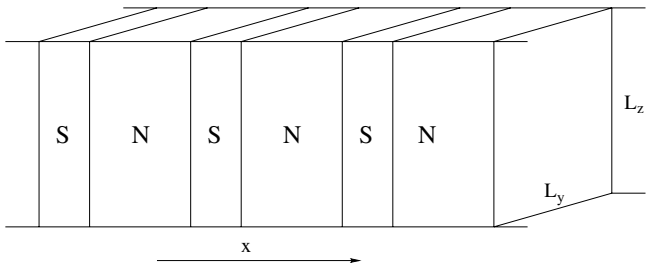

Figure 1. Illustration of an SN multilayer with finite transverse widths.

Recently [5], a powerful Green function formalism was published which unified earlier formulations [1–4] and improved upon them. First applications were made for NS, SNS, and SNSNS systems [5–7]. An important feature of these calculations was that the systems were chosen to have a finite transverse width and they were focused on particular phenomena which occur at specially chosen transverse widths. Up to now treatments have only been known for an infinite width [8–10], or if a finite width was considered it was done in a global way, in terms of the number of allowed transverse modes [4, 11, 12].

The aim of the present paper is to show applications to different SN multilayer structures, by which we understand a periodic sequence of S and N layers, extended in the x-direction, see figure 1. A set of observables is calculated, such as the local density of states (LDOS) in the S and N layers of a multilayer, and the supercurrent in the multilayer.

In section 2, we present the theory, applied to SN multilayers. In many situations, it is enough to work within the Andreev approximation (AA), which reduces to taking into account only Andreev reflections at the S/N interfaces. In section 3 we will show results derived within the AA. Exact calculations, which include ordinary reflections, are discussed in section 4, in relation with the so-called critical transverse widths, at which a new transverse mode is starting to contribute. In section 5 we present results for the supercurrent in the SN multilayers. In section 6 we study the consequences of using a self-consistently calculated gap. Finally, to complete the picture, in section 7 we take into consideration an interface potential, by this modelling a Schottky barrier. We apply a simple δ-function barrier located at the SN interface, introduced by Blonder *et al* [13].

2. Clean SN structures

The purpose of this section is to summarize first the basic ingredients of the general theory presented in [5] which we need in calculating the LDOS $\rho(x, E)$ for energies E of the order of magnitude of the gap energy and the supercurrent I. After that we show how the general theory is elaborated for applications to SN multilayers.

We study a periodic SN multilayer, which extends in the x-direction, as depicted in figure 1. In the transverse directions y and z, the system has finite size, $L_y = L_z = L_t$. We apply a Kronig–Penney superlattice model, depicted in figure 2, which means that the pair potential is

$$\Delta(x + d_S + d_N) = \Delta(x)\mathrm{e}^{\mathrm{i}\phi}$$
$$\Delta(x) = \begin{cases} \Delta & \text{if } x \in \text{S layer} \\ 0 & \text{if } x \in \text{N layer,} \end{cases} \tag{1}$$

where d_S and d_N are the thicknesses of the S and N layers respectively, and ϕ is the phase difference between two neighbouring S layers.

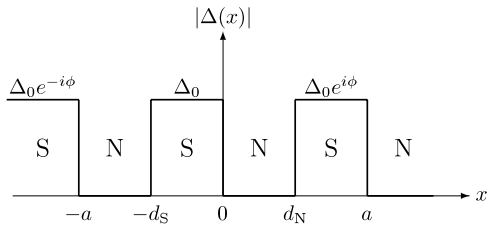

Figure 2. The Kronig–Penney model for the pair potential, used in [8].

Both quantities we want to calculate can be expressed in terms of the Green function in the following way:

$$\rho(x, E) = -\frac{2}{\pi}\frac{1}{L_y L_z}\lim_{\delta\to 0}\sum_{k_y,k_z}\mathrm{Im}\ G_{11}(x, x; k_y, k_z, E + \mathrm{i}\delta). \tag{2}$$

$$I = -2\mathrm{i}e\frac{1}{L_y L_z}\sum_{k_y,k_z}\lim_{x'\to x}\left(\frac{\partial}{\partial x'} - \frac{\partial}{\partial x}\right)kT\sum_n G_{11}(x, x'; k_y, k_z, \mathrm{i}\omega_n) \tag{3}$$

where the Green function G_{11} is the upper left element of the matrix Green function.

The Green function can be expressed in terms of a kind of wavefunction, which is the solution of the one-dimensional differential equation

$$\begin{pmatrix} \mathrm{i}\omega_n + \frac{\mathrm{d}^2}{\mathrm{d}x^2} + k_{Fx}^2 & -\Delta \\ -\Delta^* & \mathrm{i}\omega_n - \frac{\mathrm{d}^2}{\mathrm{d}x^2} - k_{Fx}^2 \end{pmatrix}\Psi(x) = 0 \tag{4}$$

where $k_{Fx}^2 \equiv \mu - k_y^2 - k_z^2$. Note that the Bogoliubov equations arise from equation (4) by substituting $\mathrm{i}\omega_n \to E$. The solution of equation (4) for the spatially dependent Δ of the multilayer (1) is built up by starting with the solution for a homogeneous superconductor, having a constant Δ_S. The wavefunction can then be written as

$$\Psi_S^{\sigma\nu}(x) = \begin{pmatrix} u_S^{\sigma}\mathrm{e}^{\mathrm{i}\phi_S/2} \\ u_S^{-\sigma}\mathrm{e}^{-\mathrm{i}\phi_S/2} \end{pmatrix}\mathrm{e}^{\mathrm{i}\sigma\nu k_S^{\sigma}x}, \tag{5}$$

with $u_S^{\sigma} = \sqrt{\mathrm{i}\omega_n + \mathrm{i}\sigma\Omega_S}$, $\mathrm{i}\Omega_S = \sqrt{(\mathrm{i}\omega_n + 0^+)^2 - \Delta_S^2}$ and the Matsubara frequencies $\omega_n = n\pi k_B T$, n taking odd integer values only. The four standard solutions are labelled with the sign indices σ and ν, that can both equal ± 1. The index σ refers to the type of the propagating particle (electron-like for $\sigma = +$ and holelike for $\sigma = -$) and the index ν indicates the direction of propagation.

In order to express the Green function in terms of $\Psi_S^{\sigma\nu}(x)$, a conjugate wavefunction is needed, namely,

$$\tilde{\Psi}_S^{\sigma\nu}(x) = \begin{pmatrix} u_S^{\sigma}\mathrm{e}^{-\mathrm{i}\phi_S/2} & u_S^{-\sigma}\mathrm{e}^{\mathrm{i}\phi_S/2} \end{pmatrix}\mathrm{e}^{\mathrm{i}\sigma\nu k_S^{\sigma}x} \tag{6}$$

(which is not the *Hermitian* conjugate), in which ν has now to be interpreted as minus the direction of propagation.

With the use of these wavefunctions, we can express the Green function for a homogeneous superconductor as

$$\mathcal{G}_S(x, x') = \sum_{\sigma} d_S^{\sigma}\Psi_S^{\sigma\mu}(x)\tilde{\Psi}_S^{\sigma,-\mu}(x'), \tag{7}$$

with $\mu = \mathrm{sgn}(x - x')$ and $d_S^{\sigma} = -\frac{1}{4\Omega_S k_S^{\sigma}}$.

2.1. A single interface and more interfaces

For a single interface, situated at the position x_j, the general form of the Green function is

$$G_{\nu j\nu' j}(x,x') = \mathcal{G}_{\nu j}(x,x')\delta_{\nu\nu'} + \sum_{\sigma\sigma'} d^{\sigma}_{\nu j} d^{\sigma'}_{\nu' j} \Psi^{\sigma\nu}_{\nu j}(x) t^{\sigma\sigma'\nu\nu'}_{\nu j\nu' j} \tilde{\Psi}^{\sigma'\nu'}_{\nu' j}(x'), \tag{8}$$

where the subscript (νj) refers to the part of the system that is on the ν side of the interface at position x_j. The first term accounts for the possible ways of propagating from x' to x without being scattered at the interface, while the second term describes the propagation via the interface.

The scattering matrix $t^{\sigma\sigma'\nu\nu'}_{\nu j\nu' j'}$ is found by applying boundary conditions at $x = x_j$. We require the continuity of the Green function and its derivative. Thus, the equation obeyed by the t-matrix is

$$\sum_{\sigma\nu} \nu d^{\sigma}_{\nu j} \Psi^{\sigma\nu}_{\nu j}(x_j) t^{\sigma\sigma'\nu\nu'}_{\nu j\nu' j} = -\nu' \Psi^{\sigma';-\nu'}_{\nu' j}(x_j). \tag{9}$$

If we consider a system with an arbitrary number of interfaces, with position coordinates $x_j < x_{j+1}$, then the scattering of the quasiparticles is described by the scattering matrices $T^{\sigma\sigma'\mu\mu'}_{\nu j\nu' j'}$. The general form of the Green function is

$$G_{\nu j\nu' j'}(x,x') = \mathcal{G}_{\nu j}(x,x')[\delta_{\nu\nu'}\delta_{jj'} + \delta_{-\nu\nu'}\delta_{j+\nu,j'}] + \sum_{\sigma\sigma'}\sum_{\mu\mu'} d^{\sigma}_{\nu j} d^{\sigma'}_{\nu' j'} \Psi^{\sigma\mu}_{\nu j}(x) T^{\sigma\sigma'\mu\mu'}_{\nu j\nu' j'} \tilde{\Psi}^{\sigma'\mu'}_{\nu' j'}(x'). \tag{10}$$

Again, imposing the boundary conditions, we obtain a Lippmann–Schwinger equation which allows us to calculate the T-matrices by means of the single-interface t-matrices

$$T^{\sigma\sigma'\nu\mu'}_{\nu j\nu' j'} = t^{\sigma\sigma'\nu\mu'}_{\nu j\mu' j}[\delta_{\mu'\nu'}\delta_{jj'} + \delta_{-\mu'\nu'}\delta_{j+\mu',j'}] + \sum_{\sigma''\nu''} t^{\sigma\sigma''\nu\nu''}_{\nu j\nu'' j} d^{\sigma''}_{\nu'' j} T^{\sigma''\sigma',-\nu''\mu'}_{\nu''\nu' j'}. \tag{11}$$

This equation expresses the idea of multiple scattering, since the matrix $T^{\sigma\sigma'\nu\mu'}_{\nu j\nu' j'}$ contains all possible processes that yield the correct final state. The first term in equation (11) accounts for the possibility that the particle is scattered once. The second term collects the processes in which the particle is scattered once due to $t^{\sigma\sigma''\nu\nu''}_{\nu j\nu'' j}$ and an arbitrary number of other times due to $T^{\sigma''\sigma',-\nu''\mu'}_{\nu''\nu' j'}$.

2.2. Periodic SN multilayers

So far we have just summarized the description given previously [5]. We will now focus on an infinite periodic SN multilayer to which the theory has not been applied yet. For an infinite multilayer, it is always possible to refer to any layer of the system by referring to an even-numbered (or an odd-numbered) interface only. This can lead to a further simplification of the Lippmann–Schwinger equation. We choose to refer to any part of the system by referring to the even interfaces. However, for the t-matrices, both even and odd interface indices need to be used.

In order to rewrite equation (11) for the present purpose, we define the following matrices:

$$\boldsymbol{T}_{jj'} \equiv \boldsymbol{D}_j \delta_{jj'} + \begin{pmatrix} T^{\sigma\sigma',-\mu\mu'}_{\mu j\mu' j'} & T^{\sigma\sigma',-\mu\mu'}_{\mu j,-\mu' j'} \\ T^{\sigma\sigma',-\mu\mu'}_{-\mu j\mu' j'} & T^{\sigma\sigma',-\mu\mu'}_{-\mu j,-\mu' j'} \end{pmatrix} \tag{12}$$

$$\boldsymbol{D}_j \equiv \begin{pmatrix} \frac{\delta_{\sigma\sigma'}\delta_{\mu\mu'}}{d^{\sigma}_{\mu j}} & 0 \\ 0 & \frac{\delta_{\sigma\sigma'}\delta_{\mu\mu'}}{d^{\sigma}_{-\mu j}} \end{pmatrix} \tag{13}$$

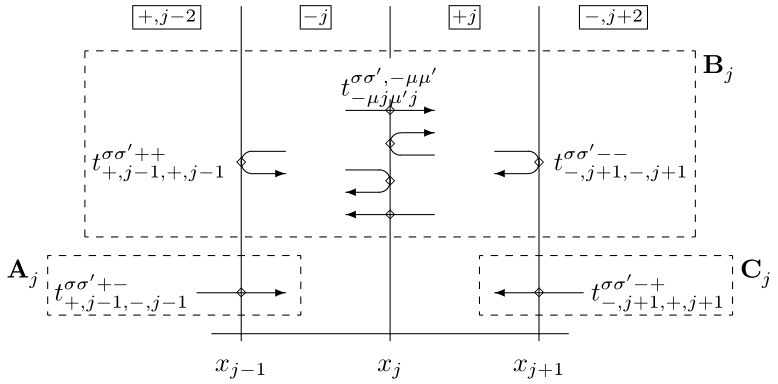

Figure 3. Schematic representation of the processes accounted for by the matrices $\boldsymbol{A}_j$, $\boldsymbol{B}_j$ and $\boldsymbol{C}_j$.

$$\boldsymbol{A}_j \equiv \begin{pmatrix} 0 & t^{\sigma\sigma',-\mu\mu'}_{-\mu,j+\mu,\mu',j+\mu} d^{\sigma'}_{-\mu',j-2}\delta_{\mu-}\delta_{\mu'-} \\ 0 & 0 \end{pmatrix} \tag{14}$$

$$\boldsymbol{B}_j \equiv \begin{pmatrix} 0 & t^{\sigma\sigma',-\mu\mu'}_{-\mu,j+\mu,\mu',j+\mu} d^{\sigma'}_{-\mu'j}\delta_{-\mu\mu'} \\ t^{\sigma\sigma',-\mu\mu'}_{-\mu j\mu' j} d^{\sigma'}_{\mu' j} & 0 \end{pmatrix} \tag{15}$$

$$\boldsymbol{C}_j \equiv \begin{pmatrix} 0 & t^{\sigma\sigma',-\mu\mu'}_{-\mu,j+\mu,\mu',j+\mu} d^{\sigma'}_{-\mu',j+2}\delta_{\mu+}\delta_{\mu'+} \\ 0 & 0 \end{pmatrix}. \tag{16}$$

All elements of these 2×2 matrices can themselves be regarded as 4×4 matrices, with the indices (σ, μ) and (σ', μ') labelling the rows and the columns, respectively. That makes $\boldsymbol{T}_{jj'}$ an 8×8 matrix that satisfies

$$\boldsymbol{A}_j \cdot \boldsymbol{T}_{j-2,j'} + (\boldsymbol{B}_j - \mathbf{1}) \cdot \boldsymbol{T}_{jj'} + \boldsymbol{C}_j \cdot \boldsymbol{T}_{j+2,j'} + \boldsymbol{D}_j \delta_{jj'} = 0. \tag{17}$$

In terms of these matrices, the system Green function (10) has the following form:

$$G_{\nu j\nu' j'}(x, x') = \mathcal{G}_{\nu j}(x, x')[\delta_{\nu\nu'}\delta_{jj'} + \delta_{-\nu\nu'}\delta_{j+\nu,j'}] + \sum_{\sigma\sigma'}\sum_{\mu\mu'} d^{\sigma}_{\nu j} d^{\sigma'}_{\nu' j'} \Psi^{\sigma\mu}_{\nu j}(x)$$
$$\times (\boldsymbol{T}_{jj'} - \boldsymbol{D}_j\delta_{jj'})^{\sigma\sigma'\mu\mu'}_{\nu j\nu' j'}(\ldots \boldsymbol{A}_j, \boldsymbol{B}_j, \boldsymbol{C}_j, \boldsymbol{A}_{j+1}, \boldsymbol{B}_{j+1}, \boldsymbol{C}_{j+1}, \ldots)\tilde{\Psi}^{\sigma'\mu'}_{\nu' j'}(x'). \tag{18}$$

All possible scattering processes are incorporated in equation (17), which expresses the content of the Lippmann–Schwinger equation. To illustrate the different processes accounted for by the $\boldsymbol{A}_j$, $\boldsymbol{B}_j$ and $\boldsymbol{C}_j$ matrices, we show a schema in figure 3.

We now turn to the periodic system. For the moment, we assume that the phase of the pair potential is the same and equal to zero in all the S layers. The periodicity allows us to simplify the problem and to rewrite equation (17). First we perform the following transformations

$$\hat{t}^{\sigma\sigma'\nu\nu'}_{\nu j\nu' j} \equiv \mathrm{e}^{\mathrm{i}\sigma\nu k^{\sigma}_{\nu j} x_j} t^{\sigma\sigma'\nu\nu'}_{\nu j\nu' j} \mathrm{e}^{\mathrm{i}\sigma'\nu' k^{\sigma'}_{\nu' j} x_j}, \tag{19}$$

$$\hat{T}^{\sigma\sigma'\nu\nu'}_{\mu j\mu' j'} \equiv \mathrm{e}^{\mathrm{i}\sigma\nu k^{\sigma}_{\mu j} x_j} T^{\sigma\sigma'\nu\nu'}_{\mu j\mu' j'} \mathrm{e}^{\mathrm{i}\sigma'\nu' k^{\sigma'}_{\mu' j'} x'_j}. \tag{20}$$

The scattering matrices with hats no longer depend on the interface positions x_j, although they still refer to the interface number, through the labels νj.

The matrices $\boldsymbol{T}_{jj'}$, $\boldsymbol{D}_j$, $\boldsymbol{A}_j$, $\boldsymbol{B}_j$ and $\boldsymbol{C}_j$ become

$$\hat{\boldsymbol{T}}_{jj'} \equiv \hat{\boldsymbol{D}}_j\delta_{jj'} + \begin{pmatrix} \hat{T}^{\sigma\sigma',-\mu\mu'}_{\mu j\mu' j'} & \hat{T}^{\sigma\sigma',-\mu\mu'}_{\mu j,-\mu' j'} \\ \hat{T}^{\sigma\sigma',-\mu\mu'}_{-\mu j\mu' j'} & \hat{T}^{\sigma\sigma',-\mu\mu'}_{-\mu j,-\mu' j'} \end{pmatrix} \tag{21}$$

$$\hat{\boldsymbol{D}} \equiv \begin{pmatrix} \frac{\delta_{\sigma\sigma'}\delta_{\mu\mu'}}{d^{\sigma}_{\mu}} e^{-i\sigma k^{\sigma}_{\mu} a_{\mu}} & 0 \\ 0 & \frac{\delta_{\sigma\sigma'}\delta_{\mu\mu'}}{d^{\sigma}_{-\mu}} e^{-i\sigma k^{\sigma}_{-\mu} a_{-\mu}} \end{pmatrix} \tag{22}$$

$$\hat{\boldsymbol{A}} \equiv \begin{pmatrix} 0 & \hat{t}^{\sigma\sigma',-\mu\mu'}_{\mu,-\mu'} d^{\sigma'}_{-\mu'} \delta_{\mu-}\delta_{\mu'-} e^{i\sigma' k^{\sigma'}_{-\mu'} a_{-\mu'}} \\ 0 & 0 \end{pmatrix} \tag{23}$$

$$\hat{\boldsymbol{B}} \equiv \begin{pmatrix} 0 & \hat{t}^{\sigma\sigma',-\mu\mu'}_{\mu,-\mu'} d^{\sigma'}_{-\mu'} \delta_{-\mu\mu'} e^{i\sigma' k^{\sigma'}_{-\mu'} a_{-\mu'}} \\ \hat{t}^{\sigma\sigma',-\mu\mu'}_{-\mu\mu'} d^{\sigma'}_{\mu'} e^{i\sigma' k^{\sigma'}_{\mu'} a_{\mu'}} & 0 \end{pmatrix} \tag{24}$$

$$\hat{\boldsymbol{C}} \equiv \begin{pmatrix} 0 & \hat{t}^{\sigma\sigma',-\mu\mu'}_{\mu,-\mu'} d^{\sigma'}_{-\mu'} \delta_{\mu+}\delta_{\mu'+} e^{i\sigma' k^{\sigma'}_{-\mu'} a_{-\mu'}} \\ 0 & 0 \end{pmatrix}. \tag{25}$$

After these transformations, and as a consequence of the periodicity, the Green function becomes dependent on the relative coordinates only, and the j-independent layer thicknesses $a_{\mu} = \mu(x_{j+\mu} - x_j)$ and $a_{-\mu} = \mu(x_j - x_{j-\mu})$ can be defined. In terms of these matrices, equation (17) now reads as

$$\hat{\boldsymbol{A}} \cdot \hat{\boldsymbol{T}}_{j-2,j'} + (\hat{\boldsymbol{B}} - \mathbf{1}) \cdot \hat{\boldsymbol{T}}_{jj'} + \hat{\boldsymbol{C}} \cdot \hat{\boldsymbol{T}}_{j+2,j'} + \hat{\boldsymbol{D}}\delta_{jj'} = 0. \tag{26}$$

This is a kind of discretized version of the original Green function equation. The general solution is

$$\hat{\boldsymbol{T}}_{jj'} = \hat{\boldsymbol{X}}^{|j-j'|/2}_{\mathrm{sgn}(j-j')} \cdot \hat{\boldsymbol{T}}_0, \tag{27}$$

where $\hat{\boldsymbol{X}}_-$, $\hat{\boldsymbol{X}}_+$ and $\hat{\boldsymbol{T}}_0$ are implicitly given by the following set of equations:

$$\hat{\boldsymbol{A}} \cdot \hat{\boldsymbol{X}}^2_- + (\hat{\boldsymbol{B}} - \mathbf{1}) \cdot \hat{\boldsymbol{X}}_- + \hat{\boldsymbol{C}} = 0 \tag{28}$$

$$\hat{\boldsymbol{A}} + (\hat{\boldsymbol{B}} - \mathbf{1}) \cdot \hat{\boldsymbol{X}}_+ + \hat{\boldsymbol{C}} \cdot \hat{\boldsymbol{X}}^2_+ = 0 \tag{29}$$

$$[\boldsymbol{A} \cdot \hat{\boldsymbol{X}}_- + (\hat{\boldsymbol{B}} - \mathbf{1}) + \hat{\boldsymbol{C}} \cdot \hat{\boldsymbol{X}}_+] \cdot \hat{\boldsymbol{T}}_0 + \hat{\boldsymbol{D}} = 0. \tag{30}$$

Note that (28) and (29) are quadratic equations. By that, for a periodic system, we can rewrite the expression of the Green function (18) in a simpler form

$$G_{\nu j\nu' j'}(x, x') = \mathcal{G}_{\nu j}(x, x')[\delta_{\nu\nu'}\delta_{jj'} + \delta_{-\nu\nu'}\delta_{j+\nu,j'}] + \sum_{\sigma\sigma'}\sum_{\mu\mu'} d^{\sigma}_{\nu j} d^{\sigma'}_{\nu' j'} \Psi^{\sigma\mu}_{\nu j}(x - x_j)$$
$$\times (\hat{\boldsymbol{T}}_{jj'} - \hat{\boldsymbol{D}}_j\delta_{jj'})^{\sigma\sigma'\mu\mu'}_{\nu j\nu' j'}(\hat{\boldsymbol{A}}, \hat{\boldsymbol{B}}, \hat{\boldsymbol{C}}) \tilde{\Psi}^{\sigma'\mu'}_{\nu' j'}(x' - x_{j'}). \tag{31}$$

The problem of calculating the LDOS or the supercurrent reduces to solving the system of quadratic matrix equations (28)–(30).

After some manipulations, one can manage to reduce the problem to solving a 2×2 matrix equation, which is equivalent to solving a system of eight simultaneous equations with real coefficients. In the appendix, we show this more explicitly.

The formalism described up to now can be extended to the situation in which the pair potentials have phase differences, that allow for currents in the multilayer to flow.

By convention, we assume that the N layer also has a phase equal to the phase of one of the two adjacent S layers. This means that the phase over a bilayer is constant and it makes a jump of ϕ at the edges between two bilayers.

Suppose the interface between two bilayers is chosen at odd j, then for even j the t-matrices obey the equation

$$\sum_{\sigma\nu} \nu d^{\sigma}_{\nu j} u^{\sigma\nu}_{\nu j} \hat{t}^{\sigma\sigma'\nu\nu'}_{\nu j\nu' j} = -\nu' u^{\sigma',-\nu'}_{\nu' j} \qquad (j \text{ even}) \tag{32}$$

while for odd interfaces a ϕ dependence remains and we are left with

$$\sum_{\sigma\nu} \nu d^{\sigma}_{\nu j} U(\nu\phi\delta_{-\nu\nu'}) u^{\sigma\nu}_{\nu j} \hat{t}^{\sigma\sigma'\nu\nu'}_{\nu j\nu' j} = -\nu' u^{\sigma',-\nu'}_{\nu' j} \qquad (j \text{ odd}), \tag{33}$$

where

$$U(\phi) \equiv \begin{pmatrix} e^{i\phi/2} & 0 & 0 & 0 \\ 0 & e^{-i\phi/2} & 0 & 0 \\ 0 & 0 & e^{i\phi/2} & 0 \\ 0 & 0 & 0 & e^{-i\phi/2} \end{pmatrix}. \tag{34}$$

3. Local density of states in SN multilayers

First we apply the theory in calculating the LDOS in the middle of one of the S or N layers. For most of the systems which will be described, the transverse width L_t is fixed to 13 bohr, the chemical potential $\mu = 0.5$ Ryd and the LDOS is normalized to the spatially constant LDOS of the bulk N material. The coupling potential V is calculated using the BCS formula

$$T_c = 1.13\omega_D e^{-1/N(\mu)V}, \tag{35}$$

where $N(\mu) = \sqrt{\mu}/4\pi$. For Al with $T_c = 1.2$ K, $\mu = 0.5$ Ryd and $\omega_D = 375$ K, we find $V = 9.516$ Ryd. For the pair potential Δ we choose a value of 0.0001 Ryd. Given the BCS relation $\Delta/k_B T_c = 1.77$, the pair function should be somewhat larger, $\Delta = 0.000\,18$ Ryd. However, we should also keep in mind the reduction of the pair function due to the finite size of the system. We will discuss this in section 6, in which we will determine the gap function self-consistently. Furthermore, many of the results we will show are not very sensitive to the precise choice for Δ.

It appears that the LDOS curves for SN multilayers look rather complicated. As a preparation to understand them, we first look at simpler systems and we postpone the treatment of SN multilayers to sections 3.2 and 3.3. In the coming subsection, we will follow the development of the LDOS for a bulk system to the LDOS for systems with a few interfaces.

3.1. From bulk superconductor to SNS system

In this subsection we will first follow the development of the LDOS for a bulk bar-shaped superconductor to the LDOS of an SN multilayer with $d_S \gg (\xi, d_N)$ and of multilayers with $d_S \gg \xi$, in which d_N becomes comparable to d_S. For the present clean systems the BCS coherence length $\xi \approx 4000$ bohr. Looking at figure 2 it is clear that a multilayer with thick S layers, such that $d_S \gg \xi$, comes close to an SNS system, particularly for $E < \Delta$.

In figure 4 we show the LDOS inside the S layer of an SN multilayer and the DOS of bulk S material. One clearly sees the singularity in the LDOS at $E = \Delta$. The non-zero DOS of the S material for $E < \Delta$ is due to the small imaginary part $i\delta$ added to the energy, $E + i\delta$. In all calculations we used $\delta \approx 0.02\Delta$. Here $d_N = 1000$ bohr and $d_S = 50\,000$ bohr, so that the presence of the N layer is just a small perturbation from a bar-shaped superconductor.

First we concentrate on the development of the LDOS for $E < \Delta$. In figure 5 we show for the same system both the LDOS inside the S and the N layers. Due to the very small N layer thickness, there is just one Andreev bound state in the N layer LDOS close to the gap value of the energy, which is broadened by δ to a peak.

Figures 6–8 show what happens to the LDOS of the SN multilayers if we increase d_N to $d_N = 2000$, 4000 and 10 000 bohr respectively. The pictures look more and more complex as we increase d_N. In the N layer LDOS we notice the appearance of more Andreev bound states at lower and lower energies. The singularity in the S layer DOS lowers, certainly due to reduced interaction of the neighbouring S layers.

The oscillations in the LDOS in all figures for $E > \Delta$ are a periodic-multilayer effect. Before discussing this band structure effect, we will first consider multilayer systems with decreasing d_S, thus making more explicit the multilayer character of the system.

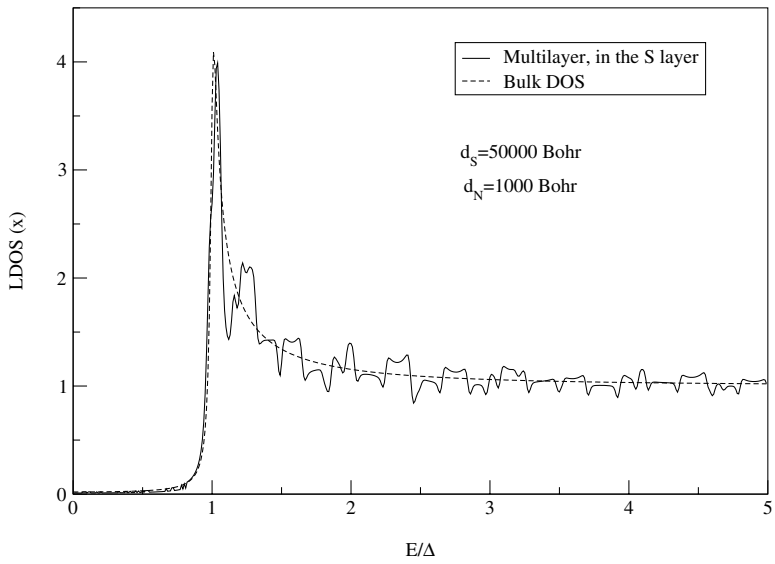

Figure 4. LDOS for an SN multilayer ($d_S = 50\,000$ bohr and $d_N = 1000$ bohr) and for a bar-shaped superconductor (dashed curve).

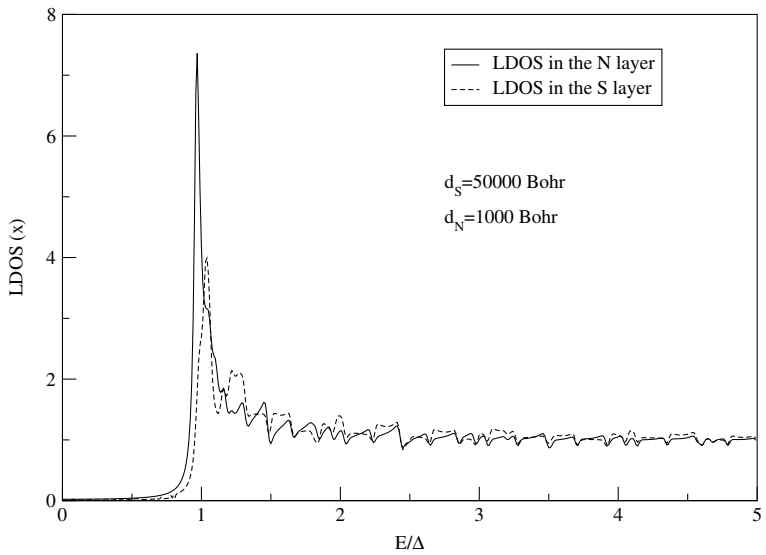

Figure 5. LDOS for an SN multilayer ($d_S = 50\,000$ bohr and $d_N = 1000$ bohr) in the N layer (solid curve) and S layer (dashed curve).

3.2. From SNS system to SN multilayer

Let us pick up the N layer LDOS from figure 8 and put it together with the LDOS of an SNS system, whose $d_N = 10\,000$ bohr. This is what we show in figure 9. The good similarity is due to the large d_S. This SN multilayer is just a perturbation of an SNS system, as we can notice from the small oscillations at energies E which are larger than the gap. Way below $E = \Delta$ the Andreev bound states curves coincide. Just below $E = \Delta$ the clear peak in the

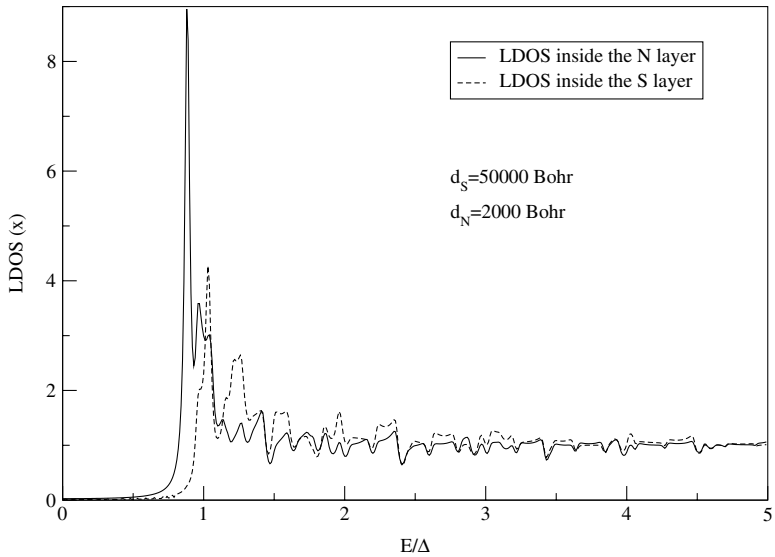

Figure 6. LDOS for an SN multilayer ($d_S = 50\,000$ bohr and $d_N = 2000$ bohr) in the N layer (solid curve) and S layer (dashed curve).

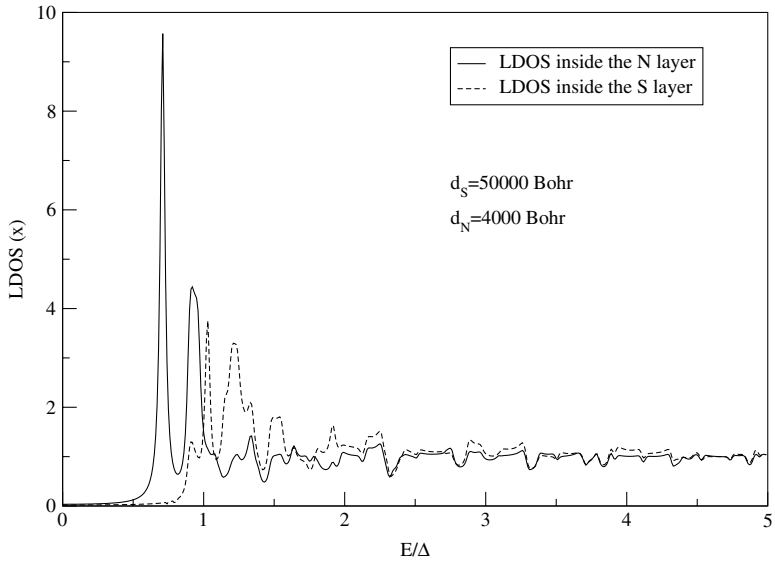

Figure 7. LDOS for an SN multilayer ($d_S = 50\,000$ bohr and $d_N = 4000$ bohr) in the N layer (solid curve) and S layer (dashed curve).

SNS system curve is smeared out in the multilayer curve, due to tunnelling interaction between the N layers.

The similarity between SNS systems and SN multilayers reduces with decreasing d_S. Multilayer features start to appear gradually in the LDOS, as we can see in figures 10 and 11.

Due to the increased tunnelling, the discrete states start to form bands, while at E larger than the gap, the oscillations are more pronounced and follow a periodicity, according to the

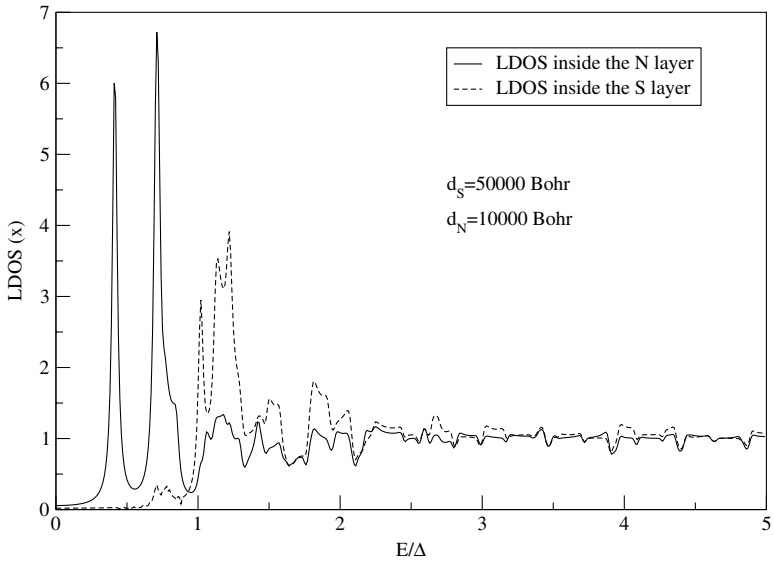

Figure 8. LDOS for an SN multilayer ($d_S = 50\,000$ bohr and $d_N = 10\,000$ bohr) in the N layer (solid curve) and S layer (dashed curve).

dispersion relations [8]

$$\begin{aligned}\cos[(k_x - k_{Fx})(d_S + d_N)] &= \cosh\frac{\sqrt{E^2 + |\Delta|^2}d_S}{2k_{Fx}}\cosh\left(\frac{Ed_N}{2k_{Fx}} + \frac{\mathrm{i}\phi}{2}\right) \\ &+ \sinh\frac{\sqrt{E^2 + |\Delta|^2}d_S}{2k_{Fx}}\sinh\left(\frac{Ed_N}{2k_{Fx}} + \frac{\mathrm{i}\phi}{2}\right) \\ \cos[(k_x + k_{Fx})(d_S + d_N)] &= \cosh\frac{\sqrt{E^2 + |\Delta|^2}d_S}{2k_{Fx}}\cosh\left(\frac{Ed_N}{2k_{Fx}} - \frac{\mathrm{i}\phi}{2}\right) \\ &+ \sinh\frac{\sqrt{E^2 + |\Delta|^2}d_S}{2k_{Fx}}\sinh\left(\frac{Ed_N}{2k_{Fx}} - \frac{\mathrm{i}\phi}{2}\right),\end{aligned} \tag{36}$$

where k_{Fx} is given by

$$k_{Fx}^2 = \mu - \left(\frac{n_y\pi}{L_t}\right)^2 - \left(\frac{n_z\pi}{L_t}\right)^2. \tag{37}$$

In figure 12 we illustrate these dispersion relations for a multilayer with $d_S = d_N = 10\,000$ bohr and two different choices for the phase difference, $\phi = 0$ and π. To make it clearer, we consider here only the $(1, 2)$-mode contribution to the LDOS. We notice the change in the succession of gaps with the phase ϕ.

Using the definition of k_{Fx}, we notice that the number of allowed modes (n_y, n_z) is limited by the condition $k_{Fx}^2 \geqslant 0$. Besides, since k_{Fx} is different for each mode, the periodicity with which there is a solution for k_x in the equations (36) is also different. For a higher mode (n_y, n_z), k_{Fx} is smaller and the frequency with which peaks and gaps in the LDOS are alternating increases. We can see this in figure 13, where we compare the contributions to the LDOS coming from different modes, at phase $\phi = 0$. As in figure 12, the system has $d_S = d_N = 10\,000$ bohr. One can easily check that by just adding the four modes' contributions one obtains the total LDOS shown in figure 14, which we are going to discuss in the following subsection.

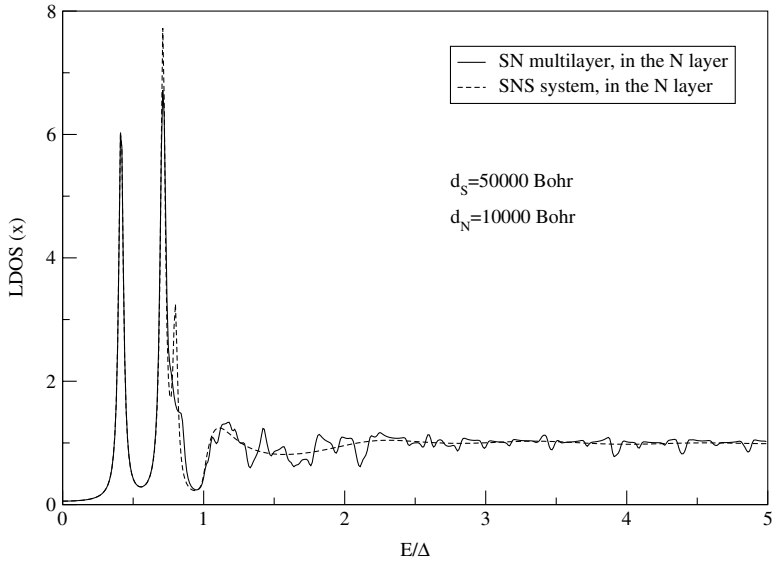

Figure 9. LDOS for an SN multilayer ($d_S = 50\,000$ bohr and $d_N = 10\,000$ bohr) and for an SNS system (dashed curve), calculated inside the N layer.

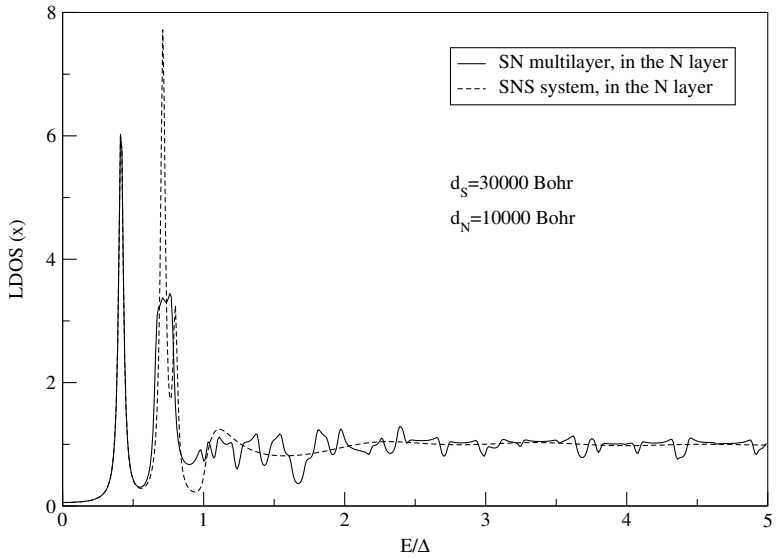

Figure 10. LDOS for an SN multilayer ($d_S = 30\,000$ bohr and $d_N = 10\,000$ bohr) and for an SNS system (dashed curve), calculated inside the N layer.

3.3. From infinite transverse size of an SN multilayer to a finite one

Now we are prepared to investigate real periodic-multilayer effects. In addition to the $\phi = 0$ result shown in figure 14 we also show the $\phi = \pi$ result for the same system in figure 15. The dispersion relations (36) are nicely illustrated in the succession of bands and gaps. This system was also studied by Tanaka and Tsukada [8]. In their figure 2(a), they describe an SN

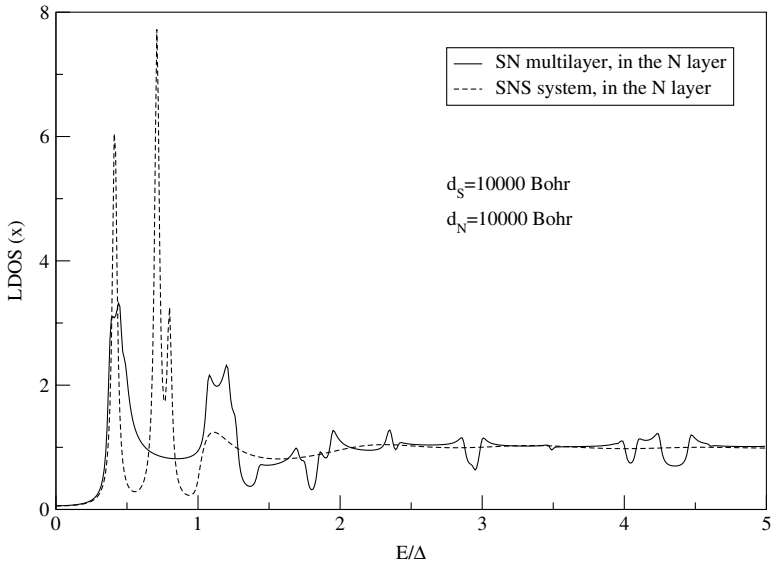

Figure 11. LDOS for an SN multilayer ($d_S = 10\,000$ bohr and $d_N = 10\,000$ bohr) and for an SNS system (dashed curve), calculated inside the N layer.

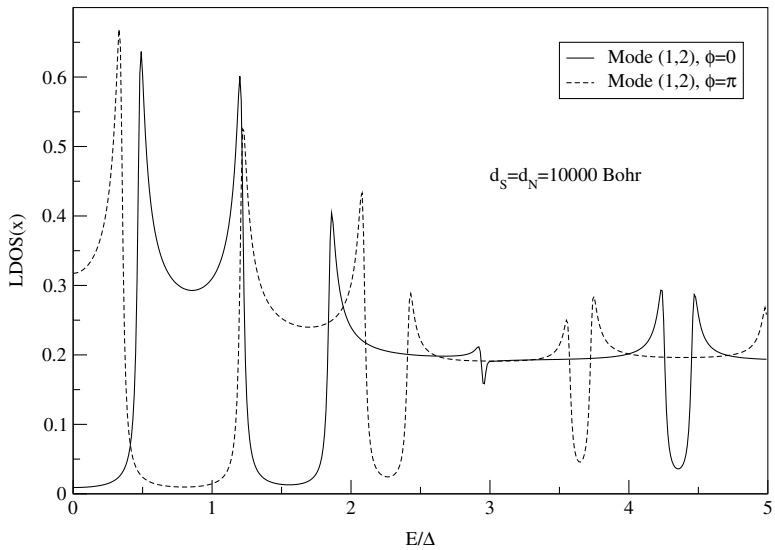

Figure 12. Contributions to the LDOS of an SN multilayer ($d_S = d_N = 10\,000$ bohr) in the middle of the N layer from the mode (1, 2), for two choices of the phase of the pair potential, $\phi = 0$ and π.

multilayer which has $d_N = d_S = 5000$ Å and $\phi = 0$, and is infinite in the transverse direction. For $E < \Delta$ the pictures look quite similar, but above the gap the LDOS in figures 14 and 15 is much less smooth than in figure 2 of Tanaka and Tsukada. However, in figure 16 we show the LDOS for a system with a larger transverse width ($L_t = 130$ bohr), and indeed, the behaviour for $E > \Delta$ has become much smoother. So we conclude that differences between our results and the results of Tanaka and Tsukada come from their use of an infinite transverse width.

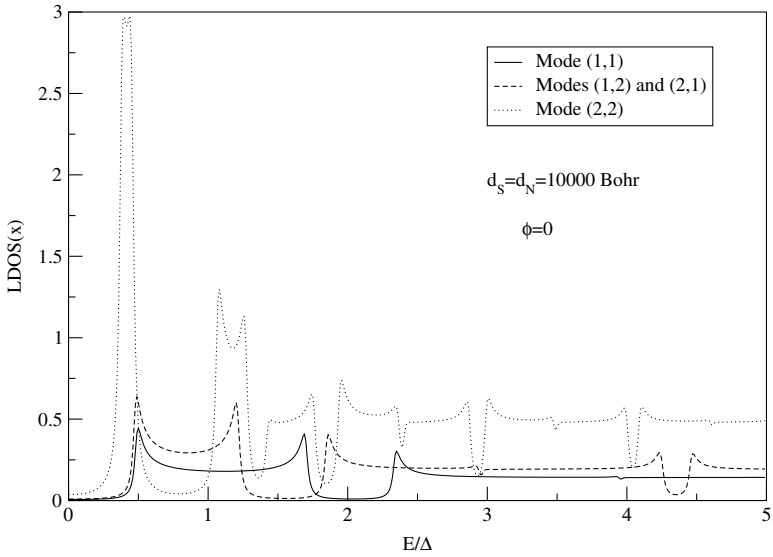

Figure 13. Contributions to the LDOS of an SN multilayer ($d_S = d_N = 10\,000$ bohr) in the middle of the N layer from the modes (1, 1), (1, 2), (2, 1) and (2, 2). The phase of the pair potential is $\phi = 0$.

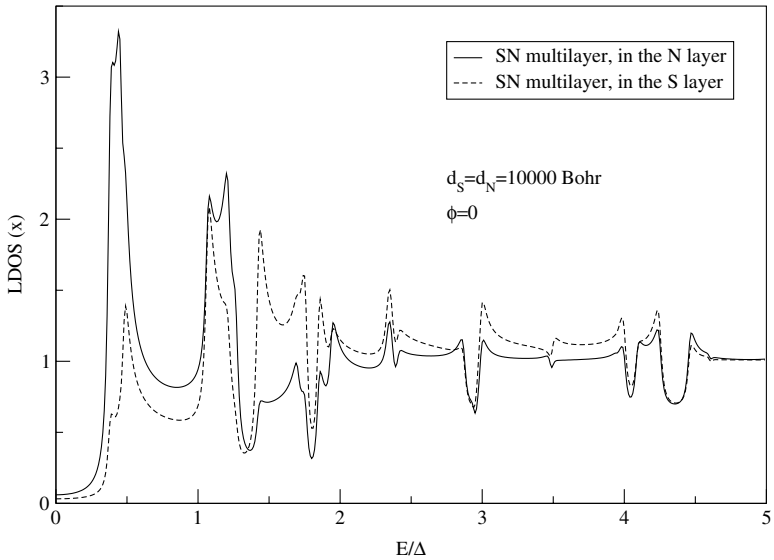

Figure 14. LDOS for an SN multilayer ($d_S = d_N = 10\,000$ bohr) in the middle of the N layer (solid curve) and S layer (dashed curve). The phase of the pair potential is $\phi = 0$.

4. Exact calculations at critical widths

In many situations, the AA gives results with an error which is estimated to be less than 0.1%. The systems which we discussed up to now satisfy the conditions for which the AA is very good. In this section, we will deal with situations in which exact calculations are necessary.

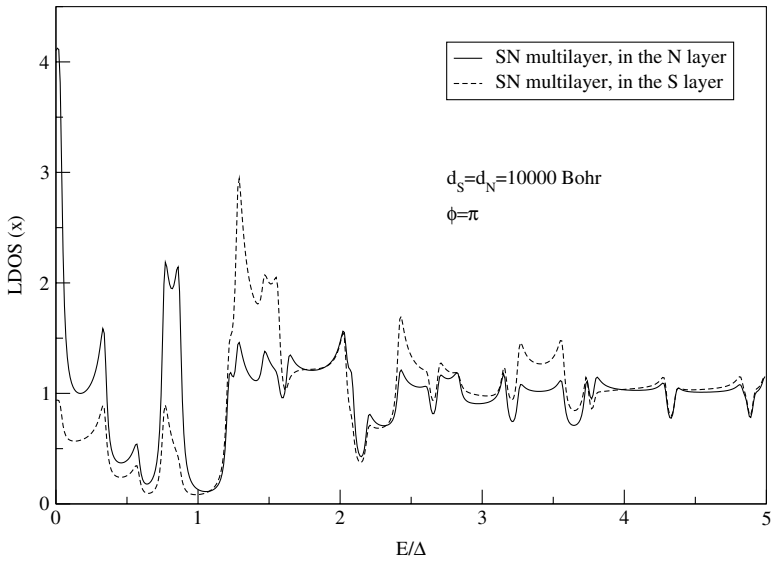

Figure 15. LDOS for an SN multilayer ($d_S = d_N = 10\,000$ bohr) in the N layer (solid curve) and S layer (dashed curve). The phase of the pair potential is $\phi = \pi$.

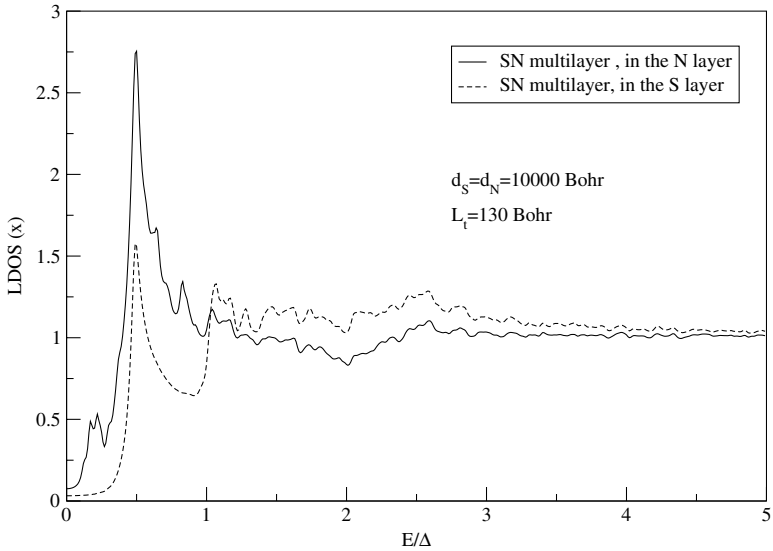

Figure 16. LDOS calculated in the N and S layers of an SN multilayer, at a higher transverse size, $L_t = 130$ bohr.

In figure 17 we show the non-normalized LDOS at $E = 5\Delta$ of a homogeneous bar as a function of the transverse width L_t. At $E = 5\Delta$, the LDOS of multilayers with the same L_t approaches a constant value, given by the homogeneous bar, as we can see in figures 4–16. We notice in figure 17 that at certain values of L_t the LDOS has steps, followed by a fast and smooth decrease. At these widths, where the condition $k_{Fx}^2 \geqslant 0$ reaches the equality, an extra mode is allowed in addition to the previous ones. The new mode has a large contribution to

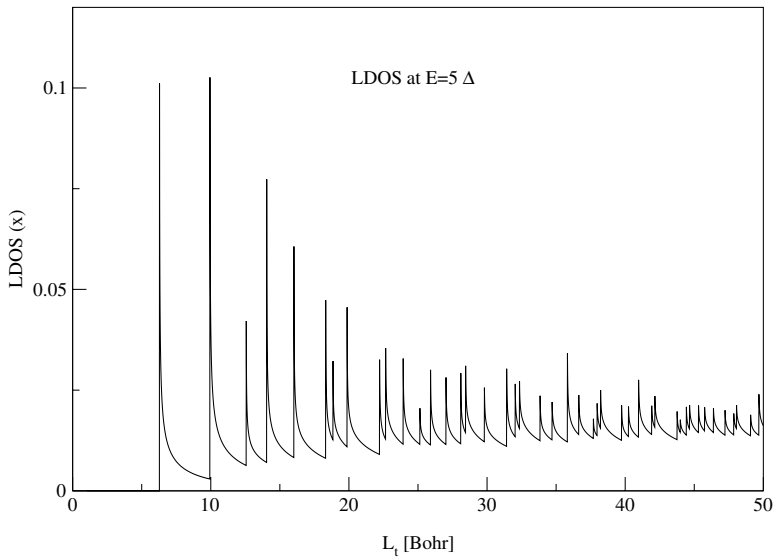

Figure 17. LDOS calculated in a bar-shaped S material, at $E = 5\Delta$, at different transverse widths.

the LDOS, explaining the step. Apparently, at smaller L_ts the steps are higher, which means that the effect of adding a new mode is larger. These values of L_t are called critical widths, and we will denote them by L_t^{cr}.

Close to the critical widths, for $0 \leqslant k_{Fx}^2 \leqslant \Delta$, the AA is no longer good. The highest modes contribute most to the LDOS, as the steps in figure 17 suggest. Besides, since k_{Fx} is very small in the dispersion relations (36), these modes will give rise to many more states than the lower modes.

As an illustration, in figure 18 we show the absolute value of the LDOS for an SN multilayer, whose $d_S = d_N = 10\,000$ bohr (as we showed in figure 14), but this time at a width $L_t = 12.566\,371$ bohr. This value of the transverse width, corresponding to the equality $k_{Fx}^2 = 0.3\Delta$ for the highest, $(2, 2)$ mode, lies very close to the critical width corresponding to $k_{Fx}^2 = 0$ and can be implemented without getting numerical problems. At this width, we calculated the LDOS at two different positions x with respect to the SN interface, inside the N layer. Although the solid and dashed curves have peaks at the same energies (the dispersion relations do not change with x), their magnitude goes up or down, depending very much on x. This is not the case within the AA, represented for comparison with a dotted curve, where peaks of the same height are situated on the energy axis at equal distance from each other. This difference between the exact and the approximate results can be explained if we make use of the definition of the LDOS,

$$\mathrm{LDOS}(\boldsymbol{r}) = \sum_n |\Psi_n(\boldsymbol{r})|^2 \delta(E - E_n). \tag{38}$$

In the AA the Andreev states with the electron moving to the right and to the left are uncoupled and are degenerate. They can be represented by plane waves, having a $\boldsymbol{r}$-independent absolute value. In the exact treatment the corresponding travelling waves are coupled and they are split into two standing waves, an odd (sinus) and even (cosinus) function. This leads to weighting factors in the expression of the LDOS which are different and position dependent. So, the lifted degeneracy in the exact calculation explains the position dependence of the LDOS illustrated in figure 18.

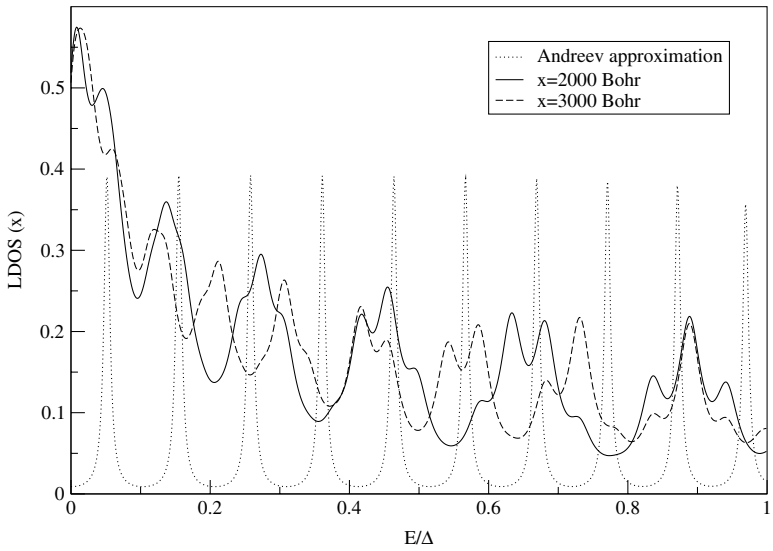

Figure 18. LDOS calculated in an SN multilayer, for a width $L_t = 12.566\,371$ bohr close to a critical width L_t^{cr}, at different positions x with respect to the S/N interface, inside the N layer. $d_N = d_S = 10\,000$ bohr. For comparison, AA is represented with dotted curve.

In order to compare multilayer results with published SNS results [5, 7], we calculated the LDOS inside the N and S layers of a multilayer with $d_N = d_S = 4000$ bohr. This is shown in figure 19 together with the SNS result. The corresponding results derived in the AA are shown in figure 20. We restricted the calculations to the highest mode's $(2, 2)$ contribution to the LDOS, at $L_t = 12.5676$ bohr. This transverse width corresponds to $k_{Fx}^2 = \Delta$ for the mode $(2, 2)$. In both figures, at energies $E < \Delta$, we do not notice any difference for the N layer. The multilayer features appear only above the gap. Besides, inside the S layer there is no contribution from the highest mode, as the corresponding states have such a small momentum k_x that, for $E < \Delta$, they are localized inside the N layer.

The features shown in this section are directly related to a fine-tuning of the transverse width. In this respect, these results are new compared to those reported by Tanaka and Tsukada [8], who have considered an infinite transverse width only.

5. Calculation of the supercurrent

This section is devoted to the supercurrent in an SN multilayer. In 1962 Josephson predicted that a supercurrent can be present in an SIS junction (Josephson junction) in the absence of an external voltage (dc Josephson effect). This current appears provided there is a difference ϕ in the phase of the pair potential between the two S layers of the Josephson junction.

$$I = I_{\max} \sin \phi. \tag{39}$$

Further, if an external potential is applied to the junction, then

$$\frac{\mathrm{d}\phi}{\mathrm{d}t} = 2eV/\hbar. \tag{40}$$

In other words, an external potential gives rise to an alternating supercurrent of frequency $f = 2eV/h$ (so-called ac Josephson effect). The quantum energy hf equals the energy of a

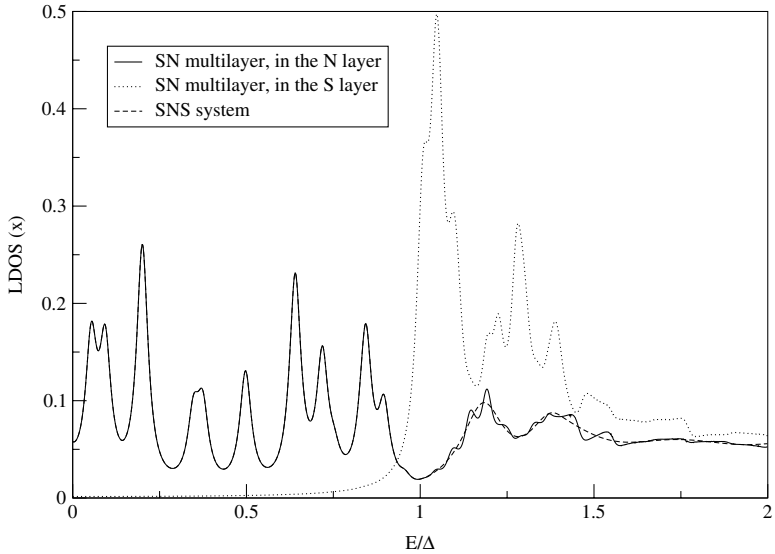

Figure 19. LDOS calculated in both S and N layers of an SN multilayer, with $d_N = d_S = 4000$ bohr, as well as in an SNS system, at a transverse width $L_t = 12.5676$ bohr.

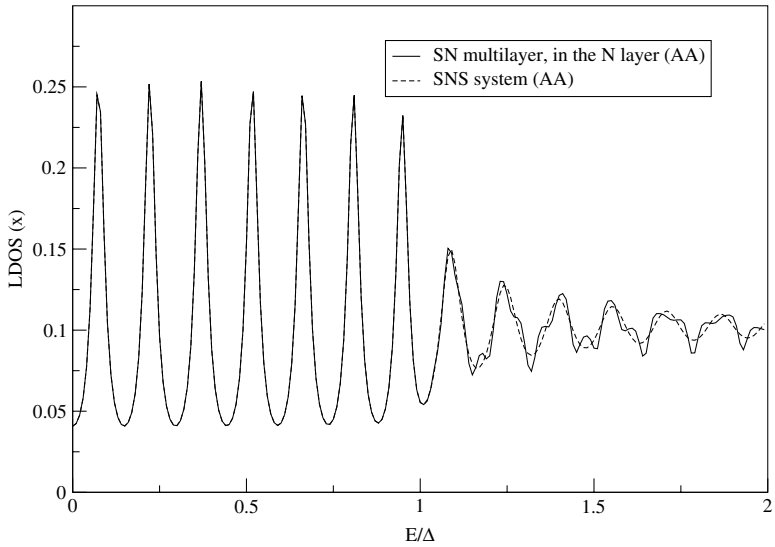

Figure 20. LDOS calculated in the AA in the N layer of an SN multilayer, with $d_N = d_S = 4000$ bohr, as well as in an SNS system, at a transverse width $L_t = 12.5676$ bohr.

Cooper pair transferred across the junction. It appears that the Josephson effect is also present in SNS junctions. We will investigate it for SN multilayers.

Using equation (3), we calculated the supercurrent I through an SN multilayer with $d_S = d_N = 10\,000$ bohr as a function of the phase difference ϕ between two consecutive S layers. Figure 21 gives the supercurrent normalized to the basic supercurrent unit $I_0 = e\Delta/\hbar$ for different choices of the transverse width L_t of the multilayer. The ϕ dependence of I is basically similar to a $\sin\phi$ dependence, as for a Josephson junction, in that it is periodic in 2π.

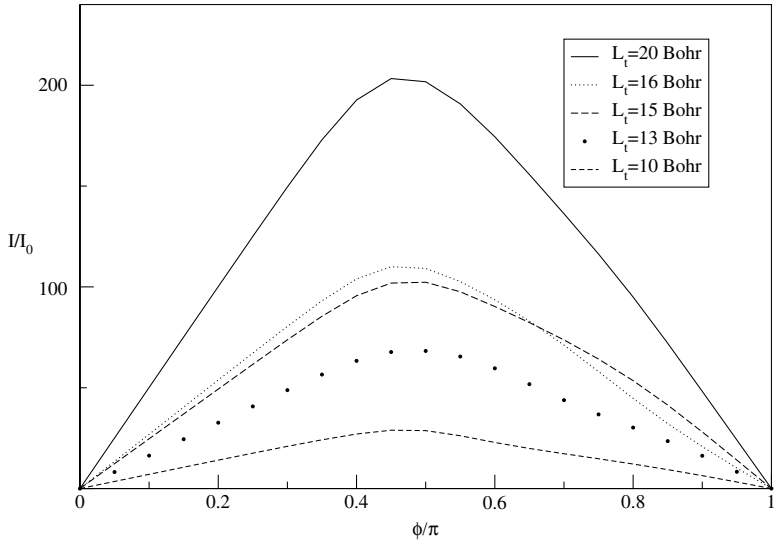

Figure 21. The dependence of the supercurrent I on the phase of the pair potential ϕ. $d_N = d_S =$ 10 000 bohr and the normalization factor $I_0 = e\Delta/\hbar$.

We notice that the supercurrent increases in magnitude with the transverse width, which makes sense, given the fact that the larger the width L_t, the more modes contribute to the current. However, a small deviation from this monotonic behaviour in the dependence of the supercurrent on the transverse widths is noticed at a larger phase, $\phi \approx 2\pi/3$. In our figure 21 we see this behaviour between the critical widths $L_t^{cr} = 14.0492$, when the mode (3, 1) starts to contribute and $L_t^{cr} = 16.0186$, when the mode (3, 2) appears. Around $\phi = 2\pi/3$, the curve corresponding to $L_t = 15$ bohr lies slightly higher than the curve for $L_t = 16$ bohr. This can be interpreted as being due to a destructive interference between the electronic contributions to the current at larger phase. This results in a small deviation from the symmetry of the sin-function dependence of the supercurrent as a function of phase. For an infinite transverse width, Tanaka and Tsukada show a similar dependence in figure 4 of their paper [8].

The way in which the transverse width influences the maximum of the supercurrent $I_{\max}$ is shown in figure 22. The monotonic increase of the supercurrent exhibits steps at each critical width. This is not surprising, since at a critical width new modes start to contribute. At the onset of this contribution, the kinetic energy of the new modes $k_F^2 - (\frac{n_{y,\max}\pi}{L_t})^2 - (\frac{n_{z,\max}\pi}{L_t})^2$ is very small and so is their contribution to the supercurrent. But with the increase of L_t, the supercurrent reaches a constant regime, until the next L_t^{cr}.

Now we fix the transverse width at $L_t = 13$ bohr and we change the layer thicknesses d_S and d_N. The results are shown in figure 23. If $d_S \gg \xi$, in which the coherence length $\xi \approx 4000$ bohr, the SN multilayer compares well to an SNS system, for which $\phi_{\max} \approx 0.8\pi$, as we will see below in discussing figure 30. At smaller values of d_S the phase $\phi_{\max}$ at which the current has a maximum shifts gradually towards lower values. Further, if the ratio between d_S and d_N is constant, the systems have approximatively the same maximum supercurrent. However, it should be noticed that all systems have the same Δ. This picture of constant $I_{\max}$ changes if the gap function is calculated self-consistently, as will be shown in section 6. With the decrease of d_N with respect to d_S, the current increases due to a better coupling between the S layers. Modifying the value of d_N does not have consequences for $\phi_{\max}$. This can be noticed if we compare the curves corresponding to $d_N = d_S = 4000$ bohr and $d_N = d_S/2 = 2000$ bohr.

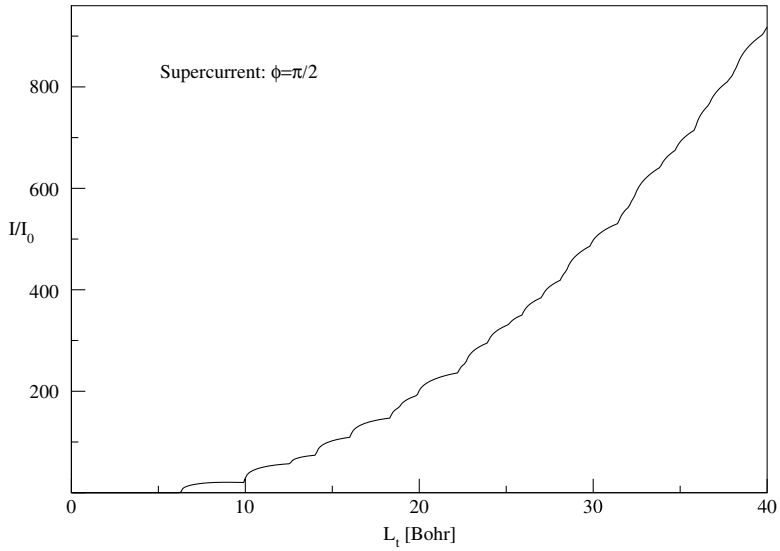

Figure 22. The dependence of the supercurrent I on the transverse length L_t. $I_0 = e\Delta/\hbar$.

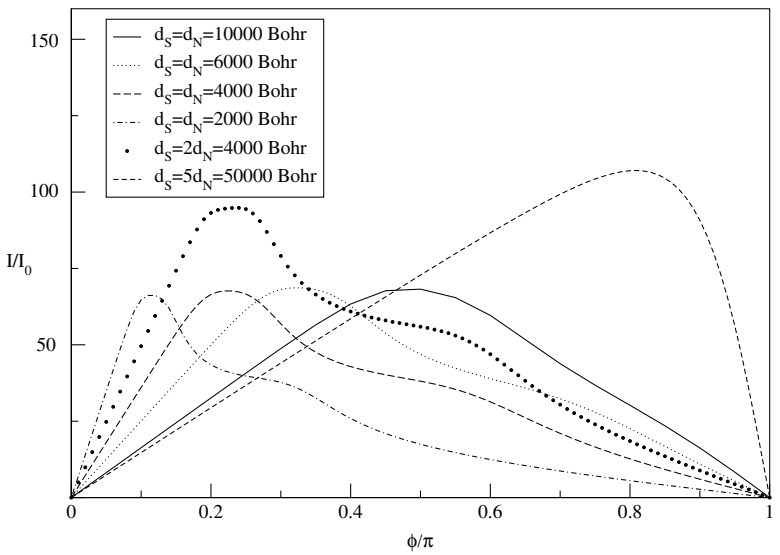

Figure 23. The dependence of the supercurrent I on d_N and d_S for $L_t = 13$ bohr. $I_0 = e\Delta/\hbar$.

6. Self-consistent calculation of the gap

The formalism described in section 2 can be applied to a self-consistent calculation of the gap function Δ. The method, which is extensively described in [5, 7], is based on the self-consistency condition

$$\Delta(x) = -k_B T V(x) \frac{1}{L_t^2} \sum_{k_y, k_z > 0} \sum_n G_{12}(x, x; k_y, k_z, \mathrm{i}\omega_n). \tag{41}$$

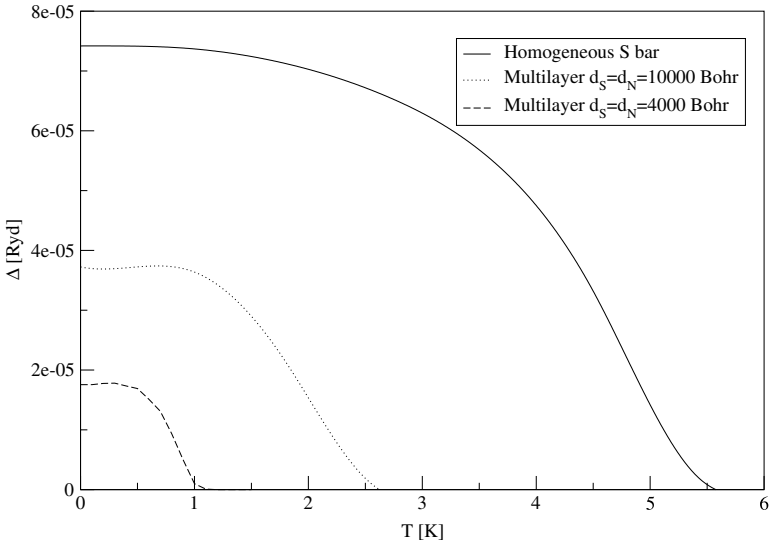

Figure 24. Self-consistent gap calculations for systems with transverse width $L_t = 30$ bohr.

Using this self-consistency condition, we can determine the absolute value of the order parameter.

The summation in equation (41) is divergent. In order to render the sum convergent, a cut-off of the summation over the Matsubara frequencies is introduced, as in the following expression:

$$\Delta(x) = -k_B T V(x) \frac{1}{L_t^2} \sum_{k_y,k_z>0} \sum_{|\omega_n|=\pi k_B T}^{\omega_D} G_{12}(x, x; k_y, k_z, \mathrm{i}\omega_n), \tag{42}$$

where ω_D is the Debye frequency. We limit the Matsubara frequency to $\omega_D = n_{\max}\pi k_B T$, where $n_{\max} = [\Theta_D/\pi T]$ and $\Theta_D = \omega_D/k_B$ the Debye temperature. As we notice, at large temperatures, $n_{\max}$ becomes small, while $d\omega_n = \omega_n - \omega_{n-1}$ is large. This gives rise to big, unphysical oscillations of the order parameter Δ with temperature T, close to T_c. We get rid of these unwanted oscillations by taking an integration, rather than a summation over ω_n. Results for a bar of transverse widths $L_t = 30$ and 100 are shown in figures 24 and 25 respectively, to which we will come back later in this section.

In addition to the integration over the Matsubara frequencies, we also investigated another cut-off method, which avoids the gap oscillations at large temperatures. An alternative way to render the summation (41) convergent is to impose the cut-off on the momenta k, instead of on the Matsubara frequencies. For a homogeneous S bar this reads

$$\Delta(x) = -\frac{k_B T V(x)}{8\pi} \frac{1}{L_t^2} \int_{k^2=\mu-k_B\Theta_D}^{\mu+k_B\Theta_D} \mathrm{d}k_x \sum_{k_y,k_z} \sum_n G_{12}(k_x, k_y, k_z, \mathrm{i}\omega_n). \tag{43}$$

More explicitly, equation (43) can be written

$$\Delta(x) = -\frac{k_B T V(x)}{8\pi} \frac{1}{L_t^2} \int_{k^2=\mu-k_B\Theta_D}^{\mu+k_B\Theta_D} \mathrm{d}k_x \sum_{k_y,k_z} \sum_n \frac{\Delta}{(\mathrm{i}\omega_n)^2 - (\mu - k_x^2 - k_y^2 - k_z^2)^2 - \Delta^2}. \tag{44}$$

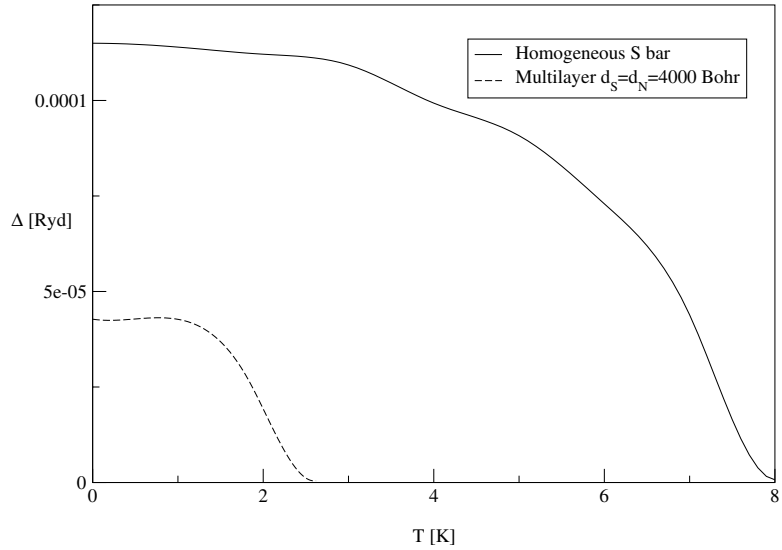

Figure 25. Self-consistent gap calculations for systems with transverse width $L_t = 100$ bohr.

We further perform the summation over the Matsubara frequencies, obtaining

$$\Delta(x) = -\frac{V(x)\Delta}{8\pi}\frac{1}{L_t^2}\int_{k^2=\mu-k_B\Theta_D}^{\mu+k_B\Theta_D} \mathrm{d}k_x \sum_{k_y,k_z} \frac{\tanh\frac{E_k}{2k_BT}}{2E_k}, \tag{45}$$

where $E_k^2 = (\mu - k_x^2 - k_y^2 - k_z^2)^2 + \Delta^2$. For bulk superconductors, both ways of rendering the integral convergent lead to the same result. However, in the case of a homogeneous S bar, we have summation over the transverse momenta k_y and k_z instead of an integration. This dramatically affects the results when k_y and k_z are large, particularly at small L_t. We can see this in the dependence of the gap Δ on the transverse width L_t, shown in figure 26. The calculation is done at $T = 0$. The dotted curve comes from a calculation with a cut-off on the Matsubara frequencies. Apparently, the latter cut-off method leads to a much more stable result than the method in which the momenta are cut off. The solid curve indeed exhibits unphysical oscillations in the gap. In addition we show a dependence $\Delta(T)$ in figure 27. This curve exhibits a greatly reduced superconductivity compared to the upper curve in figure 24 obtained by the other cut-off method. We conclude that cutting off the Matsubara frequencies leads to much more reliable results. Otadoy *et al* [5, 7] used this method to calculate the self-consistent gap for systems such as SNS and SNSNS systems. Here, we extend the application to SN multilayers. We show results for two transverse widths.

In figure 24 the temperature dependence of the gap is shown for $L_t = 30$ bohr. The solid, dotted and dashed curves represent $\Delta(T)$ for a homogeneous S bar, an SN multilayer with $d_S = d_N = 10\,000$ bohr and an SN multilayer with $d_S = d_N = 4000$ bohr respectively. As expected, the self-consistent gap decreases with the periodicity $d_S + d_N$ of the multilayer. Indeed, for a smaller d_S, the contribution to the averaged gap over the layer comes mostly from the regions close to the NS interface, where the suppression of the gap is most effective. Similarly, in figure 25 we show results for systems with $L_t = 100$ bohr. Again, one clearly sees the suppression of superconductivity by reducing the transverse width.

In addition to the results derived in section 5, in the present stage we can look to the temperature dependence of the supercurrent, by making use of the absolute value of the

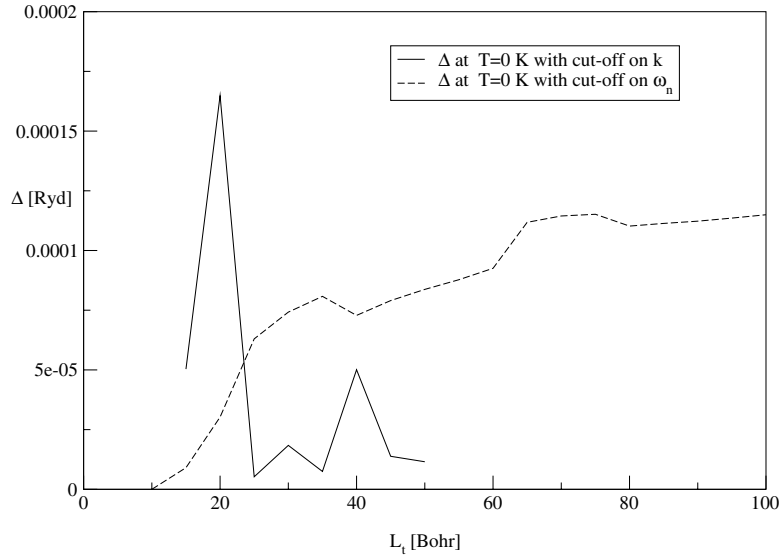

Figure 26. Self-consistent gap calculations for homogeneous S bars of different thicknesses L_t, at $T = 0$, for two different cut-off methods.

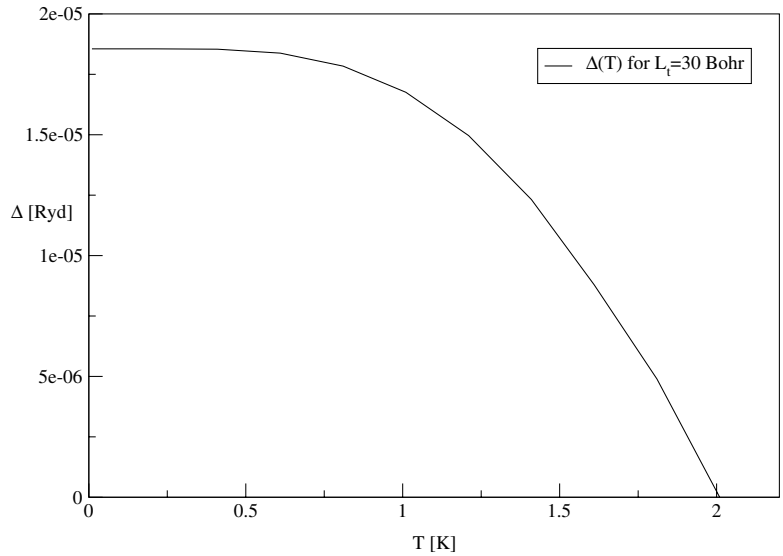

Figure 27. Self-consistent gap calculations for a homogeneous S bar of $L_t = 30$ bohr, using momentum cut-off.

order parameter, determined previously. First we show in figure 28 the phase dependence of the supercurrent for multilayers with $L_t = 30$, at different temperatures. For a given layer thickness, the peaks at different temperatures occur at the same phase. The multilayer with a smaller periodicity $d_S + d_N$ has the corresponding maximum at a lower ϕ, as we discussed in the previous section. We notice the suppression of the current with the increase of T. For the multilayer with $d_S = d_N = 10\,000$ and $L_t = 30$, we show the current–temperature dependence

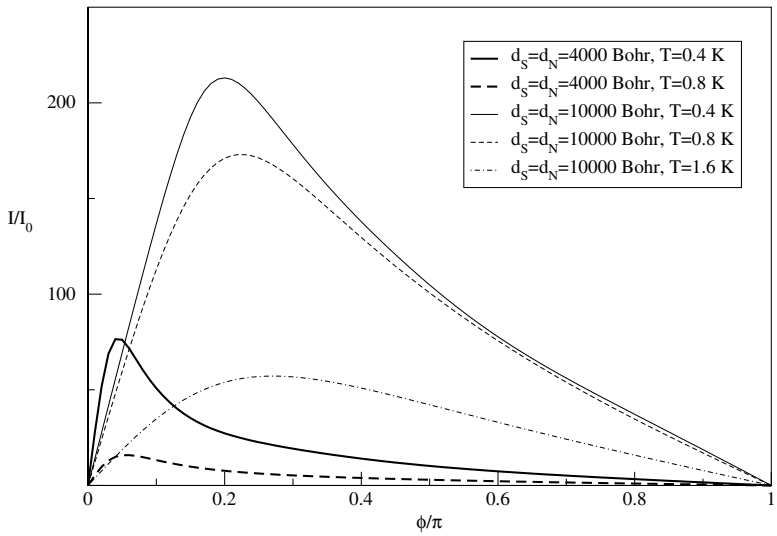

Figure 28. Phase dependence of the supercurrent I, calculated with a self-consistent gap function. $L_t = 30$ and $I_0 = e\Delta^s/\hbar$, with $\Delta^s = 0.8 \times 10^{-4}$ the self-consistent gap for the homogeneous bar at $T = 0$.

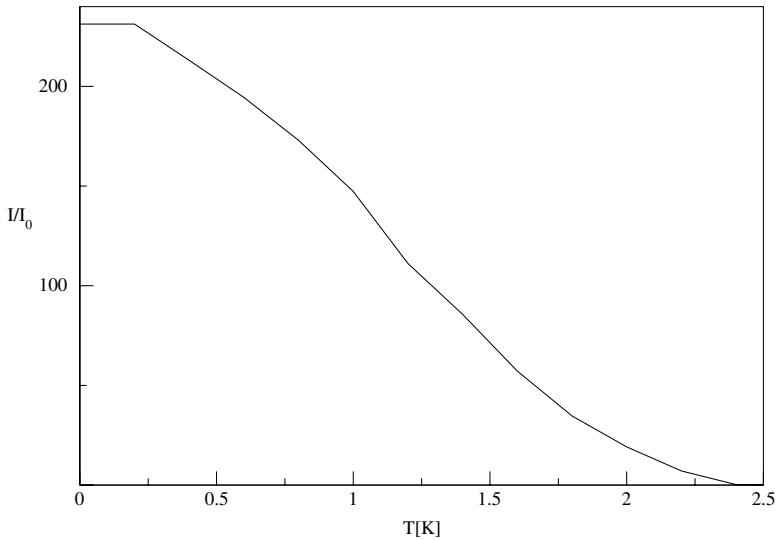

Figure 29. Self-consistent calculation of the supercurrent as a function of temperature for an SN multilayer with $d_S = d_N = 10\,000$ and $L_t = 30$. $I_0 = e\Delta^s/\hbar$ and $\Delta^s = 0.8 \times 10^{-4}$.

$I(T)$, in figure 29. The temperature at which the supercurrent becomes zero coincides with the critical temperature at which the corresponding gap function is zero, see figure 24.

Finally, we compare the phase dependence of the supercurrent for SN multilayers with corresponding results for the SNS system. In figure 30 we show results at temperature $T = 0.4$ K. The gap function in the SNS systems is equal to the homogeneous bar gap, $\Delta_{T=0.4\,\mathrm{K}} = 7.4 \times 10^{-5}$ Ryd, and it is larger than the gap inside the S layers of the SN multilayers, which takes the values $\Delta_{T=0.4\,\mathrm{K}} = 3.7 \times 10^{-5}$ Ryd for $d_S = d_N = 10\,000$ and

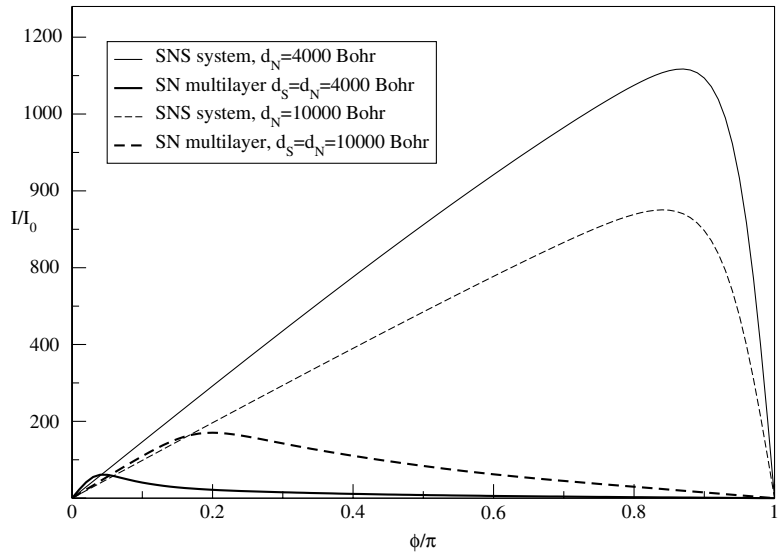

Figure 30. Self-consistent calculation of the supercurrent as a function of phase for SN multilayers with $d_S = d_N = 10\,000$ and $d_S = d_N = 4000$, and corresponding SNS systems with $d_N = 10\,000$ and $d_N = 4000$ respectively. $L_t = 30$, $I_0 = e\Delta^s/\hbar$ and $\Delta^s = 0.8 \times 10^{-4}$.

$\Delta_{T=0.4\,\mathrm{K}} = 1.7 \times 10^{-5}$ Ryd for $d_S = d_N = 4000$ respectively, as one can see in figure 24. This is why the supercurrent in the SNS systems is larger than in the SN multilayers. However, with the increase of the N layer thickness, the supercurrent in the SNS system decreases, since a thicker N layer corresponds to a weaker coupling between the two half-infinite S layers. In contrast, for the SN multilayer results shown, the S layer thickness increases as well when the N layer thickness is increased, and the supercurrent increases. In consistency with the discussion of figure 23, the phase at which the supercurrent has a maximum, $\phi_{\max}$, does not depend on the N layer thickness, and it shifts to the right with increasing d_S.

7. Interface potentials

Stimulated by recent work on the influence of interface barriers in SNS systems [14], we studied this in more detail and for SN multilayers as well. Interface barriers can come out in practice as an effect of localized disorder at the interface or as a typical oxide layer in a point contact.

A simple model of a δ-function potential at the interfaces introduced by Blonder *et al* [13] can be implemented in our formalism easily. The corresponding Hamiltonian for interfaces at positions x_j reads

$$\mathcal{H}_x \equiv -\frac{\mathrm{d}^2}{\mathrm{d}x^2} - k_{Fx}^2 + \sum_j W_j \delta(x - x_j), \tag{46}$$

where W_j is the strength of the barrier and can be estimated using the transmission coefficient of the barrier

$$\mathcal{T} \equiv \frac{1}{1 + mW^2/\hbar^2 E}. \tag{47}$$

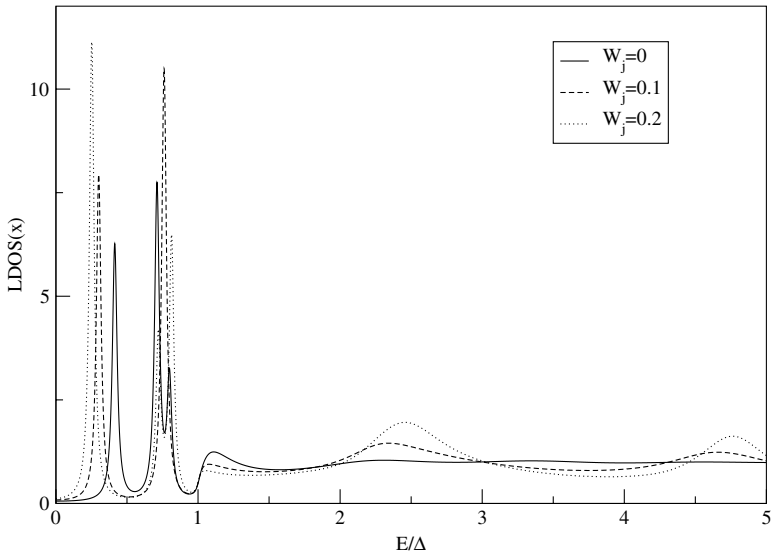

Figure 31. LDOS for an SNS system at different barrier strengths W. $d_N = 10\,000$; $L_t = 13$.

In the presence of a δ-function barrier, the wavefunction is still given by equation (4), but the boundary conditions for the Green function now read

$$\sum_{\nu} S_{\nu j} G_{\nu j \nu' j}(x_j, x') = 0, \tag{48}$$

where

$$S_{\nu j} = \begin{pmatrix} \nu & 0 & 0 & 0 \\ 0 & \nu & 0 & 0 \\ -\frac{1}{2}W_j & 0 & \nu & 0 \\ 0 & -\frac{1}{2}W_j & 0 & \nu \end{pmatrix}. \tag{49}$$

We choose $W_j = W$ the same for each SN interface.

Before applying this to SN structures, we first look at the bound states of an SNS system at different choices of the barrier strength W. In figure 31 we show the LDOS of an SNS system characterized by $d_N = 10\,000$ bohr and $L_t = 13$ bohr. In the absence of the interface potential, the SNS system LDOS has four bound states for $E < \Delta$, corresponding to the modes (1, 1), (1, 2), (2, 1) and (2, 2). Due to the fact that $L_y = L_z = L_t$, the states corresponding to the (1, 2) and (2, 1) modes are degenerate. Apparently, as we can notice, the presence of the δ-function potential favours the appearance of new bound states, due to the scattering with the interface potential. This implies that in the presence of a scattering potential even in the AA the bound states split up.

In the case of the multilayer, for which results are shown in figure 32, the deviation from the zero-potential case is even more pronounced, as the quasi-periodicity of the dispersion relations (36) is perturbed by the interface barrier. As for the SNS system, new bound states appear and complicate the picture seen in figure 14, which describes the same multilayer, but in the absence of an interface barrier.

In the limit of a large barrier strength W ($W > 1$ Ryd bohr), the S layers decouple, so that the density of states for a multilayer becomes similar to the one of an SNS system. This can be seen in figure 33, in which we show the LDOS for an SN multilayer with $d_S = d_N = 10\,000$ and $L_t = 13$, and for an SNS system with $d_N = 10\,000$. The barrier strength is $W = 10$ Ryd bohr.

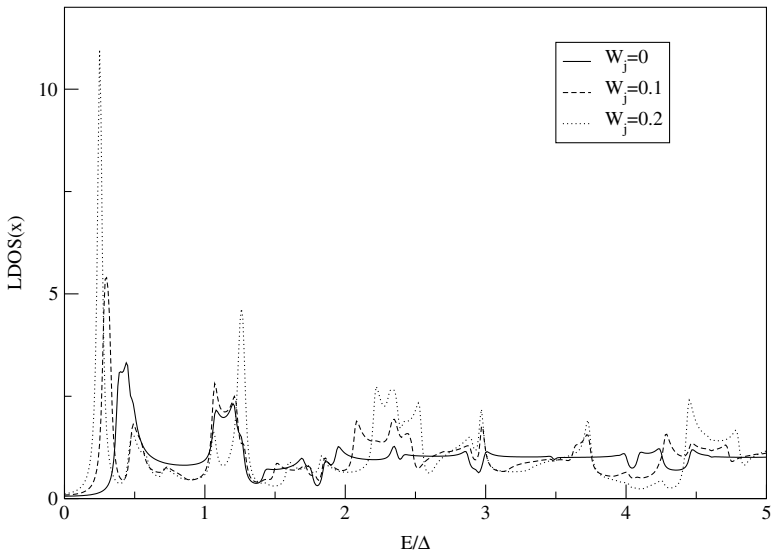

Figure 32. LDOS for an SN multilayer at different barrier strengths W. $d_S = d_N = 10\,000$; $L_t = 13$.

Compared to the strength of an S layer, which is $\Delta d_S = 1$ Ryd bohr, this interface barrier is ten times larger. At such a large strength of the barrier, in the N layer there are just bound states. To make this clearer, in figure 34 we show the contribution from each transverse mode to the LDOS of an SNS system, for energies up to ten times the gap. The peaks corresponding to the same mode (n_y, n_z) have the same height and obey the dispersion relation for a three-dimensional box,

$$E + \mu = k_x^2 + k_y^2 + k_z^2 = \left(\frac{(2n_x + 1)\pi}{d_N}\right)^2 + \left(\frac{n_y\pi}{L_t}\right)^2 + \left(\frac{n_z\pi}{L_t}\right)^2, \tag{50}$$

with $2n_x + 1 \geqslant \frac{k_{Fx}d_N}{\pi}$ and $k_{Fx} = \sqrt{\mu - \left(\frac{n_y\pi}{L_t}\right)^2 - \left(\frac{n_z\pi}{L_t}\right)^2}$. Thus, for the (1, 1) mode, the first peak has $n_x = 985$ and is situated at the energy $E = 2\Delta$, while the second peak has $n_x = 986$ and occurs at $E = 9.7\Delta$. Similarly, using equation (50) for the modes (1, 2) and (2, 1), we obtain peaks for $n_x = 726$ at $E = 3.6\Delta$ and for $n_x = 727$ at $E = 9.3\Delta$. For the mode (2, 2) we get peaks for $n_x = 288$, 289, 290, 291 and 292, at the energies $E = 0.6$, 2.9, 5.1, 7.4 and 9.7Δ respectively.

The fact that the S layers decouple in the limit of large barrier strength also has consequences on the phase dependence of the LDOS. We first show in figure 35 the LDOS of an SN multilayer without interface barrier for $\phi = 0$ and π. In this figure the solid curves of figures 14 and 15 are shown in one picture. Clearly, the features of the LDOS, already discussed in section 3, are different for the two values of the phase ϕ. However, in the presence of an interface barrier, the picture changes. In figures 36 and 37 we show the LDOS for $W = 1$ and 10 respectively. When $W = 1$, the bound states occur at almost the same energies for both phases, and for $W = 10$ the LDOS almost coincide, as a result of a complete decoupling of the successive S layers. This leads to a total suppression of the supercurrent at large values of W.

The calculated supercurrent I for an SN multilayer at different barrier strengths W is shown in figure 38. Clearly, an interface barrier diminishes the supercurrent. The stronger the

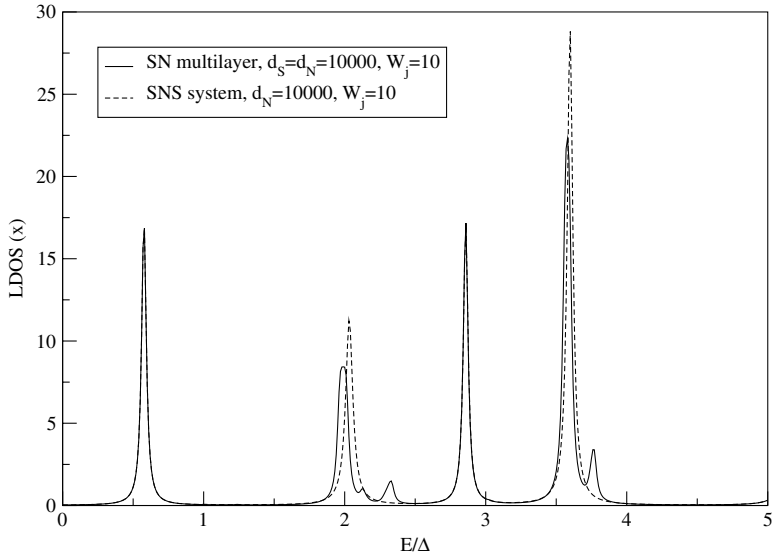

Figure 33. LDOS in the N layer of an SN multilayer and of an SNS system, at $W = 10$ Ryd bohr. $d_S = d_N = 10\,000$; $L_t = 13$.

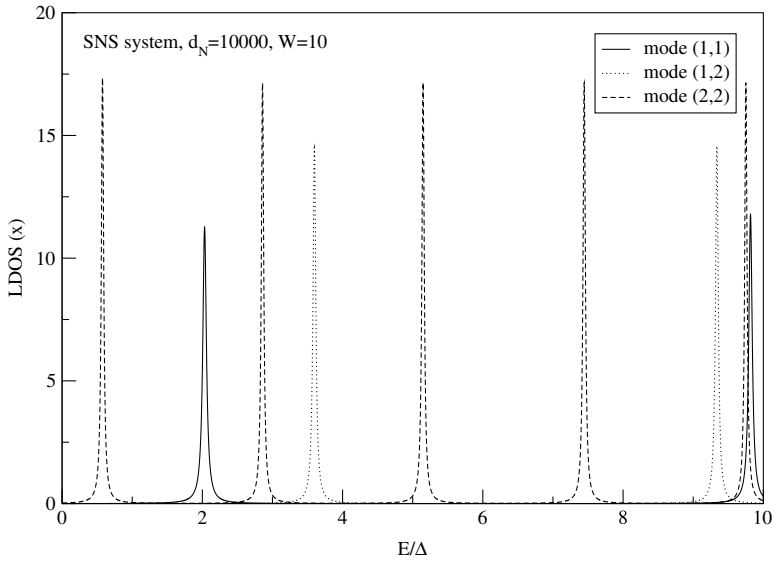

Figure 34. The contributions of the transverse modes to the LDOS of an SNS system with $W = 10$. $d_N = 10\,000$; $L_t = 13$.

barrier, the smaller is the transmission probability through the interface. For values of W larger than 2 Ryd bohr the supercurrent is completely suppressed. A similar result was obtained in the recent study mentioned above, of the Josephson current in the much simpler SNS system having several insulating barriers [14].

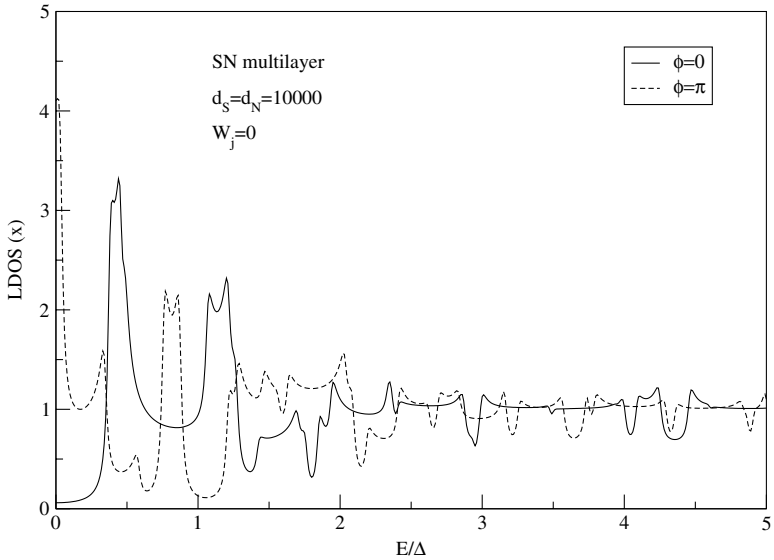

Figure 35. LDOS in the N layer of an SN multilayer at $\phi = 0$ and π, and without interface barrier. $d_S = d_N = 10\,000$; $L_t = 13$.

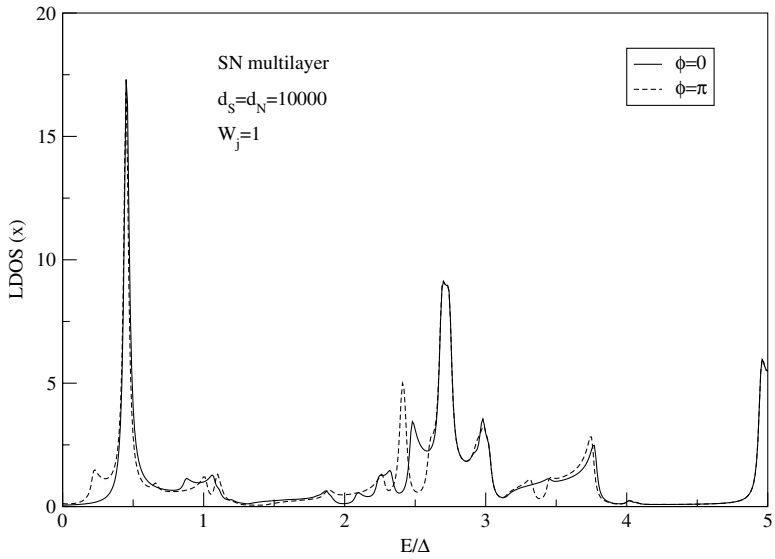

Figure 36. LDOS in the N layer of an SN multilayer at $\phi = 0$ and π, and with $W = 1$. $d_S = d_N = 10\,000$; $L_t = 13$.

8. Conclusions

In this paper we discussed SN multilayer structures. In particular we show results for periodic infinite multilayers, represented by a Kronig–Penney superlattice model. By applying a Green function formalism, we focused first on the Andreev bound states and we studied the limitations of the AA in relation to the finite transverse size of the systems.

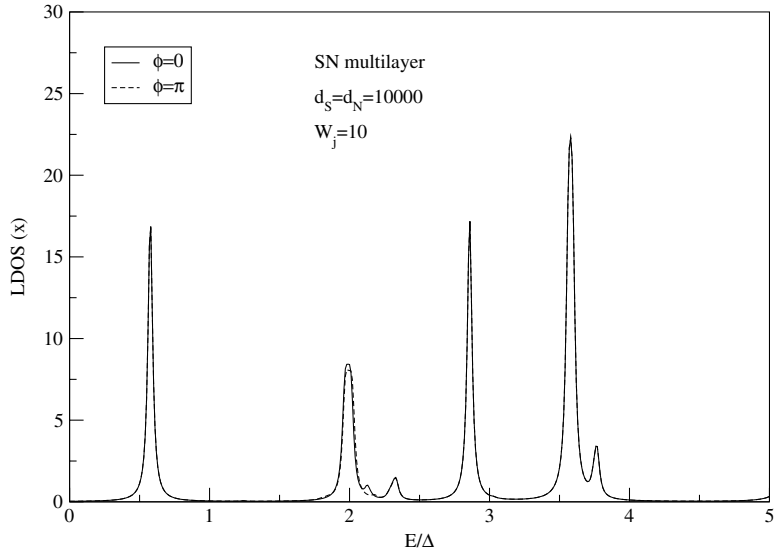

Figure 37. LDOS in the N layer of an SN multilayer at $\phi = 0$ and π, and with $W = 10$. $d_S = d_N = 10\,000$; $L_t = 13$.

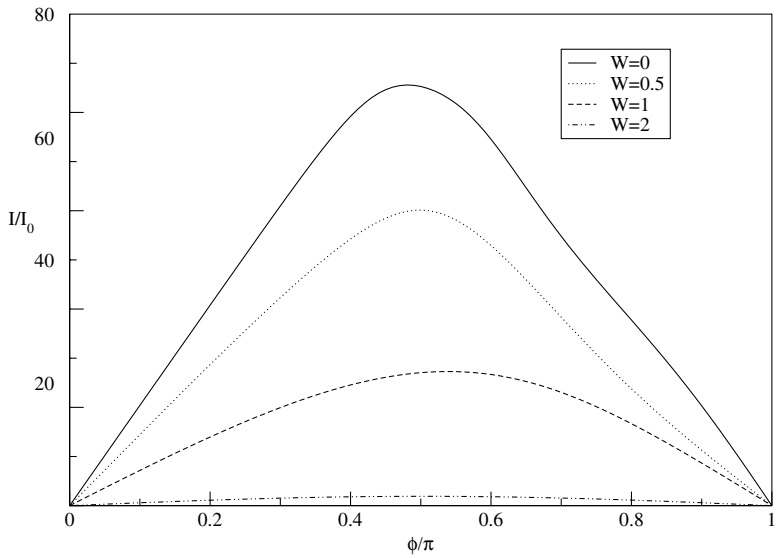

Figure 38. Supercurrent for an SN multilayer at different potentials. $d_N = 10\,000$, $L_t = 13$ and $I_0 = e\Delta/\hbar$.

Further, we calculated the supercurrent through such a periodic SN multilayer. We completed this study using a self-consistently calculated gap. Finally, including a δ-function potential at the interface, we derived results which account for possible barrier scattering at the interfaces.

The results presented in this paper are meant to increase understanding of the physics which is behind SN multilayer structures. For our purpose it is more appropriate to investigate

systems of very small transverse size because in such systems the effects of the breakdown of the AA come out most clearly. However, at the moment there are no experimental data to which we can compare. For larger systems, more accessible to experiments, the physics remains the same, but their complexity could obscure some of the fundamental aspects we are looking at.

Applications to intrinsic Josephson junctions [15] made from high-T_c S materials would require an extension of the present theory to the case of d-wave symmetry of the order parameter.

Appendix. The matrices $\hat{A}$, $\hat{B}$, and $\hat{C}$

In this appendix we show the structure of equations (28)–(30) more explicitly. The matrices $\hat{\boldsymbol{A}}$ and $\hat{\boldsymbol{C}}$ are highly singular and, due to this, the solutions of equations (28) and (29) are sparse matrices, which can be written

$$\hat{\boldsymbol{X}}_- = \begin{pmatrix} \hat{0} & \hat{0} & \hat{x}_-^{13} & \hat{0} \\ \hat{0} & \hat{0} & \hat{x}_-^{23} & \hat{0} \\ \hat{0} & \hat{0} & \hat{x}_-^{33} & \hat{0} \\ \hat{0} & \hat{0} & \hat{x}_-^{43} & \hat{0} \end{pmatrix} = \begin{pmatrix} \hat{0} & \hat{0} & \begin{pmatrix} X_-^{15} & X_-^{16} \\ X_-^{25} & X_-^{26} \end{pmatrix} & \hat{0} \\ \hat{0} & \hat{0} & \begin{pmatrix} X_-^{35} & X_-^{36} \\ X_-^{45} & X_-^{46} \end{pmatrix} & \hat{0} \\ \hat{0} & \hat{0} & \begin{pmatrix} X_-^{55} & X_-^{56} \\ X_-^{65} & X_-^{66} \end{pmatrix} & \hat{0} \\ \hat{0} & \hat{0} & \begin{pmatrix} X_-^{75} & X_-^{76} \\ X_-^{85} & X_-^{86} \end{pmatrix} & \hat{0} \end{pmatrix} \tag{A.1}$$

and

$$\hat{\boldsymbol{X}}_+ = \begin{pmatrix} \hat{0} & \hat{0} & \hat{0} & \hat{x}_+^{14} \\ \hat{0} & \hat{0} & \hat{0} & \hat{x}_+^{24} \\ \hat{0} & \hat{0} & \hat{0} & \hat{x}_+^{34} \\ \hat{0} & \hat{0} & \hat{0} & \hat{x}_+^{44} \end{pmatrix} = \begin{pmatrix} \hat{0} & \hat{0} & \hat{0} & \begin{pmatrix} X_+^{17} & X_+^{18} \\ X_+^{27} & X_+^{28} \end{pmatrix} \\ \hat{0} & \hat{0} & \hat{0} & \begin{pmatrix} X_+^{37} & X_+^{38} \\ X_+^{47} & X_+^{48} \end{pmatrix} \\ \hat{0} & \hat{0} & \hat{0} & \begin{pmatrix} X_+^{57} & X_+^{58} \\ X_+^{67} & X_+^{68} \end{pmatrix} \\ \hat{0} & \hat{0} & \hat{0} & \begin{pmatrix} X_+^{77} & X_+^{78} \\ X_+^{87} & X_+^{88} \end{pmatrix} \end{pmatrix}. \tag{A.2}$$

Substituting these matrices into equations (28) and (29), we can reduce the set to solving two quadratic matrix equations for the 2×2 complex matrices $\hat{x}_-^{33}$ and $\hat{x}_+^{44}$.

$$\hat{x}_-^{33} = \begin{pmatrix} X_-^{55} & X_-^{56} \\ X_-^{65} & X_-^{66} \end{pmatrix} \tag{A.3}$$

and

$$\hat{x}_+^{44} = \begin{pmatrix} X_+^{77} & X_+^{78} \\ X_+^{87} & X_+^{88} \end{pmatrix}. \tag{A.4}$$

This appears to be equivalent to solving a system of eight simultaneous equations with real coefficients. Mathematically, one can never predict the number of solutions. We solve this system numerically, by applying Newton's method, which requires an initial guess of the solution. Since we know that the solution is close to the AA, we give as an initial guess a diagonal matrix, namely the unitary matrix. This leads us to the physical solutions for $\hat{\boldsymbol{X}}_-$ and $\hat{\boldsymbol{X}}_+$ which, by using equation (30), allows the calculation of the $\hat{\boldsymbol{T}}_0$ matrix, which we need for the $\hat{\boldsymbol{T}}_{jj'}$ matrix (27) and the Green function (31). Finally, we are able to make use

of the expressions (2) and (3) and calculate the LDOS and the supercurrent of a periodic SN multilayer.

In the AA some matrix elements are zero and further simplifications can be made. By neglecting the ordinary reflections of the quasiparticles at the SN interfaces, some of the $\hat{t}$-matrices are equal to zero. This results in a simpler form for the matrices $\hat{\boldsymbol{A}}$ and $\hat{\boldsymbol{C}}$

$$\hat{\boldsymbol{A}} = \begin{pmatrix} 0 & 0 & 0 & 0 \\ 0 & 0 & 0 & \hat{a}_{24} \\ 0 & 0 & 0 & 0 \\ 0 & 0 & 0 & 0 \end{pmatrix}, \tag{A.5}$$

where

$$\hat{a}_{24} = \begin{pmatrix} \hat{t}_{-+}^{+++-} d_{+j}^{+} \mathrm{e}^{-\mathrm{i}k_{+j}^{+}a_{+}} & \hat{t}_{-+}^{+-+-} d_{+j}^{-} \mathrm{e}^{\mathrm{i}k_{+j}^{-}a_{+}} \\ \hat{t}_{-+}^{-++-} d_{+j}^{+} \mathrm{e}^{-\mathrm{i}k_{+j}^{+}a_{+}} & \hat{t}_{-+}^{---+} d_{+j}^{-} \mathrm{e}^{\mathrm{i}k_{+j}^{-}a_{+}} \end{pmatrix} = \begin{pmatrix} \hat{t}_{-+}^{+++-} d_{+j}^{+} \mathrm{e}^{-\mathrm{i}k_{+j}^{+}a_{+}} & 0 \\ 0 & \hat{t}_{-+}^{---+} d_{+j}^{-} \mathrm{e}^{\mathrm{i}k_{+j}^{-}a_{+}} \end{pmatrix} \tag{A.6}$$

and

$$\hat{\boldsymbol{C}} = \begin{pmatrix} 0 & 0 & \hat{c}_{13} & 0 \\ 0 & 0 & 0 & 0 \\ 0 & 0 & 0 & 0 \\ 0 & 0 & 0 & 0 \end{pmatrix}, \tag{A.7}$$

and

$$\hat{c}_{13} = \begin{pmatrix} \hat{t}_{+-}^{++-+} d_{-j}^{+} \mathrm{e}^{-\mathrm{i}k_{-j}^{+}a_{-}} & \hat{t}_{+-}^{+--+} d_{-j}^{-} \mathrm{e}^{\mathrm{i}k_{-j}^{-}a_{-}} \\ \hat{t}_{+-}^{-+-+} d_{-j}^{+} \mathrm{e}^{\mathrm{i}k_{-j}^{+}a_{-}} & \hat{t}_{+-}^{----+} d_{-j}^{-} \mathrm{e}^{-\mathrm{i}k_{-j}^{-}a_{-}} \end{pmatrix} = \begin{pmatrix} \hat{t}_{+-}^{++-+} d_{-j}^{+} \mathrm{e}^{-\mathrm{i}k_{-j}^{+}a_{-}} & 0 \\ 0 & \hat{t}_{+-}^{----+} d_{-j}^{-} \mathrm{e}^{-\mathrm{i}k_{-j}^{-}a_{-}} \end{pmatrix}. \tag{A.8}$$

In consequence, the solutions $\hat{x}_{-}^{33}$ and $\hat{x}_{-}^{44}$ then have a diagonal form.

$$\hat{x}_{-}^{33} = \begin{pmatrix} X_{-}^{55} & 0 \\ 0 & X_{-}^{66} \end{pmatrix} \tag{A.9}$$

and

$$\hat{x}_{+}^{44} = \begin{pmatrix} X_{+}^{77} & 0 \\ 0 & X_{+}^{88} \end{pmatrix}. \tag{A.10}$$

This allows us to decouple the equations for X_{-}^{55} and X_{-}^{66} into two quadratic equations which can be solved directly. The same holds for $\hat{x}_{+}^{44}$. Combining the two possible solutions for X_{-}^{55} and X_{-}^{66} with the two possible solutions for X_{+}^{77} and X_{+}^{88}, one obtains four mathematical solutions for $\hat{\boldsymbol{X}}_{-}$ and $\hat{\boldsymbol{X}}_{+}$. Two of the solutions are complementary and lead to a zero value for the LDOS. Using the other two solutions, one gets either the positive physical value for the LDOS, or the same value with the opposite sign. We use this criterion to distinguish the physical solution from the four mathematically possible solutions.

References

[1] McMillan W L and Rowell M 1969 *Superconductivity* ed R D Parks (New York: Dekker) p 561
McMillan W L 1968 *Phys. Rev.* **175** 537
McMillan W L 1968 *Phys. Rev.* **175** 559
[2] Ishii C 1972 *Prog. Theor. Phys.* **47** 1464
Ishii C 1970 *Prog. Theor. Phys.* **44** 1525
[3] Furusaki A and Tsukada M 1991 *Solid State Commun.* **78** 299
Furusaki A and Tsukada M 1990 *Physica* B **165/166** 967
[4] Furusaki A, Takayanagi H and Tsukada M 1992 *Phys. Rev.* B **45** 10563
[5] Koperdraad R T W, Otadoy R E S, Blaauboer M and Lodder A 2001 *J. Phys.: Condens. Matter* **13** 8707
[6] Blaauboer M, Koperdraad R T W, Lodder A and Lenstra D 1996 *Phys. Rev.* B **54** 4283

[7] Otadoy R E S and Lodder A 2002 *Phys. Rev.* B **65** 024521
[8] Tanaka Y and Tsukada M 1991 *Phys. Rev.* B **44** 7578
[9] Stojkovic B P and Valls O T 1994 *Phys. Rev.* B **50** 3374
[10] Miller P and Freericks J K 2001 *J. Phys.: Condens. Matter* **13** 3187
[11] Beenakker C W J 1991 *Phys. Rev.* B **67** 3836
[12] Chtchelkatchev N M, Lesovik G B and Blatter G 2000 *Phys. Rev.* B **62** 3559
[13] Blonder G E, Tinkham M and Klapwijk T M 1982 *Phys. Rev.* B **25** 4515
[14] Galaktionov A V and Zaikin A D 2002 *Phys. Rev.* B **65** 184507
[15] Kleiner R and Müller P 1997 *Physica* C **293** 156